Agricultural and Forest Meteorology 232 (2017) 332–348

Contents lists available at ScienceDirect

Agricultural and Forest Meteorology

journal homepage: www.elsevier.com/locate/agrformet

Water use in a riparian cottonwood ecosystem: Eddy covariance measurements and scaling along a river corridor

Lawrence B. Flanagan[a,*], Trina E. Orchard[a], Gordon S.J. Logie[b], Craig A. Coburn[b], Stewart B. Rood[a]

[a] Department of Biological Sciences, University of Lethbridge, Water & Environmental Science Building 4401 University Drive, Lethbridge, Alberta, T1K 3M4, Canada

[b] Department of Geography, University of Lethbridge, Water & Environmental Science Building 4401 University Drive, Lethbridge, Alberta, T1K 3M4, Canada

ARTICLE INFO

Article history:
Received 4 April 2016
Received in revised form 15 July 2016
Accepted 30 August 2016

Keywords:
Leaf area index
Penman-Monteith equation
Phenology
Populus spp
Stomatal conductance
Water-use efficiency

ABSTRACT

The survival of riparian forests depends on water input from their adjacent rivers. There are multiple, additional demands on river water that threatens to reduce the water supply, prompting the question, how much water must be left flowing within a river to sustain the native riparian ecosystems? To address this, we made eddy covariance measurements of riparian cottonwood forest evapotranspiration (ET) in a representative site and used remote sensing and the Penman-Monteith equation to up-scale ET along the 171 km river corridor from the Oldman River Dam to Lethbridge, Alberta. Our study was conducted in two growing seasons with contrasting weather conditions, including one with over-bank flooding (2014). Measured cumulative forest ET from May-September (2014: 451 ± 90 mm; 2015: 411 ± 18 mm) was very similar in the two years despite contrasting May-September cumulative precipitation input (2014: 362 mm; 2015: 181 mm). Integrated over the 56 km^2 area of riparian forest along the Oldman River corridor, the cumulative forest ET during May-September was 19.1 million m^3 (339 mm/season), about 0.9% of the average cumulative Oldman River discharge during 2008–2013. Cottonwood forest ET during May-June was less than 1% of average river flow rates during 2008–2013, but the ratio of ET to average river flow rate increased markedly to peak values of 4–5% in late July and early August. Our analysis indicated that the water-use rates of riparian cottonwood forests were high, even for a broad-leaf deciduous forest functional type, particularly given the modest leaf area index (1.4 m^2 m^{-2}) we measured for riparian forests along the Oldman River corridor. The high ET rates were possible because of tree access to alluvial groundwater to support transpiration. Our ET measurements and calculations provided perspective on riparian forest water use in relation to precipitation inputs and total river discharge, knowledge that is important for successfully managing the multiple demands on river water use.

1. Introduction

In most regions world-wide, rivers provide the primary surface water supplies for human uses including agricultural irrigation, and domestic, municipal and industrial consumption (Oki and Hanae, 2006; Vörösmarty et al., 2010). Rivers also support rich and biodiverse aquatic (instream) and riparian (streamside) ecosystems that contribute many valued environmental services (Naiman et al., 2005). These riverine ecosystems are dependent upon sufficient instream flows and this prompts the fundamental questions, how much water must be left flowing within a river to sustain the native ecosystems and conversely, how much water can be withdrawn for human use (Richter and Richter, 2000; Stromberg, 2001)?

To answer these questions and optimize river resource management, it is essential to understand the water supplies and demands within a watershed. Mass balance river basin models are developed and these characterize the water supply as provided by the natural, seasonal river inflows, and then consider the multiple human withdrawals, along with considerations for

* Corresponding author at: Department of Biological Sciences, University of Lethbridge 4401 University Drive Lethbridge, T1K 3M4 Alberta, Canada.
E-mail address: larry.flanagan@uleth.ca (L.B. Flanagan).

http://dx.doi.org/10.1016/j.agrformet.2016.08.024
0168-1923/

flow trapping and storage with dams and reservoirs (Sauchyn et al., 2016). A fundamental weakness in these models is the incomplete understanding of water use by the natural ecosystems along the river corridor. This information gap is especially problematic for semi-arid ecoregions, including the prairies, shrub-steppe and semi-desert zones, since in these areas, the rivers are 'losing streams' where water infiltrates from the river into the adjacent alluvial groundwater. The deep-rooted phreatophytic trees subsequently uptake and transpire substantial water volumes from this floodplain groundwater, but the magnitude and seasonality of floodplain forest water use and the proportional contributions from river water versus local precipitation are poorly understood (Scott et al., 2000, 2003, 2004; Wang and Dickinson, 2012).

Most of the rivers of the South Saskatchewan River Basin in southern Alberta are dammed and have regulated river flows (Schindler and Donahue, 2006; Rood et al., 2005, 2008). In the past, alterations of the river flow patterns associated with dams have caused considerable damage to riparian forests for two reasons (Rood et al., 1995, 2003a, 2005; Williams and Cooper, 2005). First, the dams reduce the magnitude of peak spring river flows and floods that create newly exposed sediments along the meandering river courses, which in turn, provide habitats for cottonwood seedling establishment without competition from other tall vegetation (Scott et al., 1997, 1999). Without the high spring flows, the cottonwood trees are unable to regenerate, because their seedlings cannot survive and develop in the shaded understory of mature forests or with other competing vegetation. Second, the dammed rivers normally only release very low water flows in the later portions of the summer (late June through September) after the natural peak in river flow that occurs in early June. The low stream flow in late summer occurs during the time of warmest air temperatures and high solar radiation input that can lead to drought stress and death of mature cottonwood trees in these riparian forest ecosystems (Rood et al., 2003a, 2005, 2008, 2013).

While it is clear that riparian forest ecosystems are reliant on the natural river flow regime they evolved with (Poff et al., 1997), it is impractical and even impossible to completely restore natural flow patterns on dammed and regulated rivers. As a practical alternative, however, it should be possible to develop procedures for a regulated river flow pattern (a functional flow pattern) that could still sustain healthy river ecosystems, but also allow for significant water withdrawal for important human uses (Rood et al., 2005). Recent examples of the implementation of the functional flows concept on the Bridge River (British Columbia, Canada) and Truckee River (Nevada, USA) have demonstrated that carefully managed river flows can restore severely degraded floodplain riparian forests (Rood et al., 2003b, 2005; Hall et al., 2009). Despite the significant success of these implementations of the functional flows concept, the new river flow patterns were applied without knowledge of the magnitude of the actual water requirements of the associated riparian forest ecosystems. This limits the water manager's ability to fine-tune the approach and to plan for altered river flow patterns and riparian forest water use in the future under climate change.

This study was undertaken to characterize the water use by a typical riparian forest in a northern prairie zone, and undertake spatial up-scaling to estimate the subsequent influence on river flows in a heavily allocated river system, the Oldman River. Our analyses involved eddy covariance flux measurements and upscaling based on remote sensing estimates of ecosystem leaf area index. The findings will contribute to the understanding of the eco-physiological function of riparian forests, and work towards resolving the largest current information gap for river basin water balance models (Nagler et al., 2005; Doody et al., 2015; Sauchyn et al., 2016).

2. Materials and methods

2.1. Study site description

Our main study site was in the Helen Schuler Nature Reserve (HSNR), a natural riparian cottonwood forest within the Oldman River valley at Lethbridge, Alberta, Canada (49.702°N, 112.863°W, elevation 928 m; Fig. 1). This riparian forest consists of the following tree species: prairie cottonwood (*Populus deltoides*), narrow-leaf cottonwood (*Populus angustifolia*), balsam poplar (*P. balsamifera*); or the closely related and almost indistinguishable black cottonwood, (*P. trichocarpa*); and their interspecific hybrids (Gom and Rood, 1999; Rood et al., 2014). Average (±SD, n = 60) tree height was 18 ± 5 m and tree diameter at breast height (1.35 m) was 37 ± 15 cm. The average (±SD; n = 33, 10 m × 10 m plots) tree density was 276 ± 300 trees per hectare. The understory of the forest consisted of grasses and other herbaceous plants plus a range of small shrubs, such as wolf willow (*Elaeagnus commutata*), silver buffaloberry (*Shepherdia argentea*), and wild rose (*Rosa acicularis*). The mean annual (1981–2010) temperature for Lethbridge was 5.9 °C and average annual precipitation was 380.2 mm (Canadian Climate Normals, Environment Canada; climate.weather.gc.ca/climate_normals/).

2.2. Leaf area index measurements at the HSNR

Leaf area index (LAI) was measured for the HSNR cottonwood canopy using the LAI-2000 (LI-COR Lincoln, NE, USA) and the Tracing Radiation and Architecture in Canopies (TRAC) (Leblanc et al., 2002) instruments. Two LAI-2000 instruments were employed to measure the LAI of the canopy. One LAI-2000 was placed on a tripod in a large open area of the cottonwood forest. It was used to collect measurements of incoming radiation with no interference from the cottonwood tree canopy. This was set to automatically measure unobstructed diffuse radiation at 30 s intervals. The second LAI-2000 was carried through the woodland along pre-determined transects to measure incoming radiation below the tree canopy. The 90° view caps were affixed to each instrument. At the start of each set of transect measurements, several measurements were taken simultaneously with the two LAI-2000 instruments side by side. These measurements were used to check the inter-calibration of the instruments while post-processing the data. The LAI-2000 measurements were conducted in the evening near sunset under diffuse illumination conditions.

The Tracing Radiation and Architecture in Canopies (TRAC) instrument was used to measure the canopy clumping index throughout the cottonwood forest along pre-determined transects. TRAC measurements were conducted in the mid-afternoon under clear, sunny skies by walking the instrument along each transect at a continuous, slow pace. The transect orientation and timing of the measurements were planned to result in a solar zenith angle between 30° and 60°, and with the Sun approximately perpendicular to the instrument path, following recommended practices (Leblanc and Chen, 2001; Leblanc et al., 2002). The clumping index was used to correct the results obtained from the LAI-2000, which does not account for within branch clumping (Leblanc and Chen, 2001; Chen et al., 2006). Tree LAI measurements were made every two weeks throughout the 2014 growing season (May-October).

Eq. (1) was used to calculate tree LAI from measurements of the LAI-2000, (Chen et al., 2006):

$$LAI = \frac{(1 - \alpha_w) \cdot L_e \cdot \gamma_E}{\Omega_E} \quad (1)$$

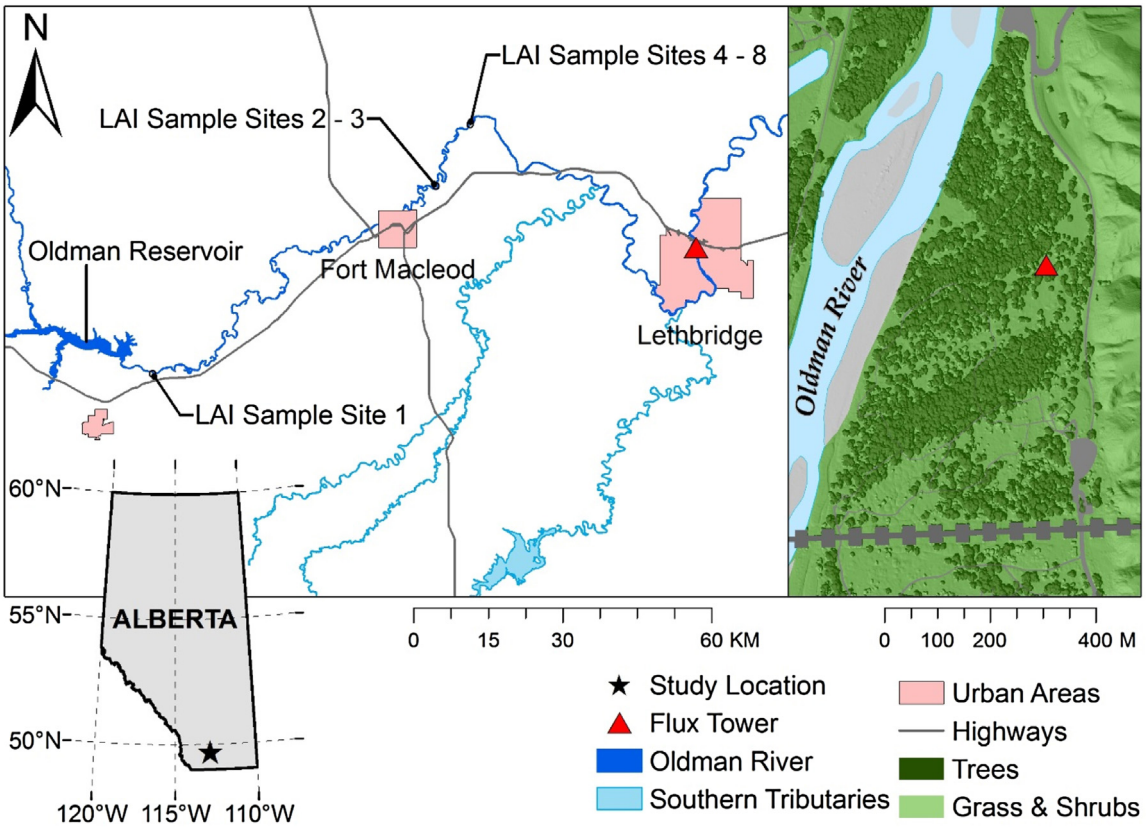

Fig. 1. Map of the Oldman River in southern Alberta, Canada including the flux tower location in Lethbridge and the LAI sample sites distributed along the river (left panel). The panel on the right shows a false color image based on an air photograph of the flux tower study site in Lethbridge.

where L_e is the effective LAI as measured by the LAI-2000 ($m^2\ m^{-2}$); γ_E is the leaf-to-shoot area ratio, where γ_E is 1 for broadleaf deciduous trees; Ω_E is the clumping index as measured using the TRAC ($\Omega_E = 0.93$ at this site); α_w is the woody-to-total leaf area ratio and was determined using the method described in Serbin et al. (2013).

$$\alpha_w = \frac{W}{L_e \frac{\gamma_E}{\Omega_E}} \quad (2)$$

where W is the woody surface area ($m^2\ m^{-2}$) or effective LAI measured with the LAI-2000 after leaf senescence had occurred. A value of 0.3 was used for W, which was experimentally determined after leaves had fallen from the trees in late fall of 2014.

Senescent tree leaves were collected in litter traps, in order to estimate peak tree LAI for comparison with measurements made using the LAI-2000 and TRAC instruments. A total of 19 laundry baskets (with areas of either 0.195 m^2 or 0.213 m^2), were randomly placed throughout the cottonwood forest to collect leaf litter. Litter was collected at two-week intervals starting in mid-September and continuing until late October when leaves had fully senesced. Collected litter was dried and the LAI of the collected litter was calculated as the product of the dry weight of the collected litter and the average leaf area/dry mass (measured on separately collected leaves), divided by the basket collection area.

Measurements of tree canopy LAI were added to the understory plant LAI obtained through destructive sampling in order to determine the total LAI for the forest. The one-sided leaf area per unit ground area of the understory plants at the HSNR was measured by harvesting, every two weeks, all vegetation rooted within a 20 × 50 cm frame. The total green leaf area of the harvested plants was measured using a leaf area meter (LI-3100C, LI-COR). This was done for the first half of the growing season until peak biomass was observed. Subsequently, a regression between green biomass and measured LAI was used to calculate LAI until the conclusion of the growing season from biomass harvest measurements. Four sampling locations were used to capture the variability observed in understory vegetation throughout the HSNR site.

2.3. Meteorological and eddy covariance flux measurements

A telescoping aluminum instrumentation tower (22.5 m tall, Model T-75HD, Aluma Tower Company Inc., Vero Beach, FL, USA) was installed at the HSNR site. The tower supported a variety of instruments for meteorological and eddy covariance measurements. An air temperature and relative humidity probe (HMP45C (Vaisala Inc.), Campbell Scientific, Inc., Logan, Utah, USA) inserted within a naturally ventilated radiation shield (41002, Gill Multi-Plate Radiation Shield, R.M. Young Company, Traverse City, Michigan, USA) was mounted at a height of 1 m. Net radiation was measured at a height of 22.5 m by a net radiometer (NR Lite, Kipp & Zonen, Delft, The Netherlands). Incoming photosynthetically-active photon flux density (PPFD) was measured at 22.5 m with a quantum sensor (LI-190SA, LI-COR Inc., Lincoln, Nebraska, USA). Soil temperature and soil moisture content were measured with soil thermocouples (105T, Campbell Scientific) and soil water reflectometers (CS616, Campbell Scientific), respectively, at depths below the surface of 100, 150, 200 and 250 cm. A site-specific calibration was developed to convert the period measurements of the water content reflectometers to volumetric moisture content. Three soil heat flux plates (REBS HFT3.1, Radiation and Energy Balance Systems, Seattle, WA, USA) were installed a depth of 5 cm. Atmospheric pressure was measured with an analogue barometer (Vaisala PTB101B, Campbell Scientific) A tipping-bucket rain gauge (CS700, Campbell Scientific) was used to measure total precipitation recorded in 30-min intervals. With the exception of the rain

gauge, all meteorological sensors were scanned at 5-s intervals and recorded as half-hourly means by a data logger (CR23X, Campbell Scientific). Any missing meteorological data was gap-filled using measurements made with similar instruments at the Lethbridge grassland eddy covariance site, which was 5.7 km distant from the cottonwood forest site (Flanagan et al., 2002; Flanagan and Atkinson, 2011). Cumulative precipitation was monitored with a weighing gauge (T-200B, Geonor Inc., Netherlands) located at the Lethbridge grassland flux site.

The eddy covariance (EC) technique (Baldocchi, 2014) was used to measure net ecosystem fluxes of CO_2, water vapour (or latent heat (*LE*)) and sensible heat (*H*). The EC system consisted of a three-dimensional sonic anemometer-thermometer (SAT; CSAT3, Campbell Scientific), used to measure wind velocity and direction (the instrument was oriented to the west at 22 m height), as well as temperature fluctuations, and a fast response, enclosed infra-red gas analyzer (IRGA; LI7200, LI-COR), used to simultaneously measure changes in CO_2 and H_2O molar densities. Air was pulled through the IRGA at a flow rate of 14 L min^{-1} by the associated LI-COR Flow Module via a 1 m length of Dekabon tubing with the tubing inlet mounted on the bottom support arm of the CSAT3 bottom transducers. Output signals from the SAT and IRGA were sampled at a frequency of 10 Hz by the associated LI-COR Analyzer Interface Unit and recorded on a storage drive. The EC system was operational during the growing season months of 2014 (May–October) and 2015 (May–August), although flux data was not collected during the period of over-bank flooding of Oldman River in June 17-July 1, 2014 and due to LI-7200 instrument malfunction during July 28-August 22, 2014. Power was supplied to the meteorological and eddy covariance sensors by an array of 6 V deep-cycle batteries that were charged by six 70 W solar panels.

Processing of high-frequency EC data was performed with EddyPro software (Version 5.2.1, LI-COR). Ecosystem fluxes of CO_2, H_2O, and *H* were calculated as the mean covariance of vertical wind velocity and scalar fluctuations. Coordinate rotations were performed to align the mean vertical velocity measurements normal to the mean wind streamlines prior to scalar flux calculations. A storage term was added to the calculated CO_2 fluxes for the determination of net ecosystem CO_2 exchange (NEE) and was estimated using the single level measurements of CO_2 concentration with the IRGA. The EC tower was located near the center on the north-south axis, and near (within 80 m) the eastern boundary of the HSNR site. This resulted in a uniform fetch of approximately 400 m in both the north and south directions from the tower, and approximately 300 m directly west of the tower. Data collected while the wind originated from the east in the direction sector between 45−135° was associated with grassland vegetation and sloped terrain outside the cottonwood forest and was removed before any analyses were completed.

We conducted an analysis to determine a level of turbulence (as indicated by friction velocity, u_*) required for acceptable nighttime CO_2 flux measurements by the EC system. Measured u_* values from the HSNR were sorted from their lowest to highest values using data from July when the canopy was at its maximum LAI and photosynthetic capacity. The u_* values (and associated nighttime NEE values) were averaged into 0.03 m s^{-1} bins ranging from 0.0–1.0 m s^{-1}. To determine the turbulence threshold, a range of possible thresholds were tested following the general procedures recommended by Aubinet et al. (2012). From this analysis we determined the u_* threshold to be 0.39 m s^{-1}.

A flux footprint analysis was conducted using the model of Kljun et al. (2004) calculated within the EddyPro software. The output from the footprint predictions gave X_{peak}, the horizontal distance (m) from the EC tower with the peak contribution to the measured fluxes, and $X_{90\%}$, the horizontal distance (m) from the EC tower within which 90% of measured fluxes originate, under the particular set of meteorological conditions input into the model. For EC data collected between 6:30–19:30 h at the HSNR site during July 2015 after the friction velocity threshold (0.39 m s^{-1}) screening was completed, the average (± SD) X_{peak} distance was 120 ± 5 m, while $X_{90\%}$, was calculated to be 330 ± 26 m. Therefore, the estimated surface contribution to the vast majority of the measured turbulent fluxes originated from within the HSNR cottonwood forest, when wind was from all directions except the excluded wind direction sector 45–135°.

As an additional assessment of the quality of the eddy covariance data, we calculated a check on the ecosystem energy balance by plotting the sum of latent and sensible heat fluxes (*y* value – see equations below) as a function of the available energy input (difference between net radiation and soil heat flux, *x*-value – see equations below). This analysis was done using all 30-min EC flux data and associated meteorological measurements collected in July of 2014 and July 2015, after first screening out data from the excluded wind sectors, data below the friction velocity threshold, and data collected during rain periods. The ordinary least-squares linear regression equations calculated for these data plots were: July 2014, $y = 0.907\,x + 43.8$, $r^2 = 0.794$; July 2015, $y = 1.005\,x + 41.0$, $r^2 = 0.854$. This represented very high quality energy balance closure for this cottonwood forest ecosystem (Wilson et al., 2002; Stoy et al., 2013).

2.4. Growing season carbon budget calculations for the HSNR

Mean diurnal patterns (bin-averages by time of day) of NEE (negative values indicate net uptake of CO_2 by the ecosystem), photosynthetic photon flux density (PPFD) and air temperature (*T*) were calculated for data from two-week periods or monthly periods during May-September depending on the available flux data. Data from the mean diurnal trends were then fitted to the following equation:

$$\mathrm{NEE} = -\frac{A_{max}\alpha PPFD}{A_{max} + \alpha PPFD} + R_{10}Q_{10}^{\left(\frac{T-10}{10}\right)} \quad (3)$$

where A_{max} is the maximum gross ecosystem photosynthesis (μmol m^{-2} s^{-1}) at infinite PPFD (μmol m^{-2} s^{-1}); α is the initial slope of the ecosystem photosynthesis light-response curve or the apparent light-use efficiency (mol CO_2 mol^{-1} photons); R_{10} is total ecosystem respiration rate (TER) at 10 °C (μmol m^{-2} s^{-1}); Q_{10} is the temperature sensitivity coefficient for TER for a 10° change in temperature; and *T* is air temperature (°C). Non-linear, least squares regressions were used to calculate estimates of A_{max}, α, R_{10} and Q_{10} parameters using Matlab software (R2014a, The Mathworks Inc., Natick, MA, USA). The calculations were done with the parameters bound over the following ranges: A_{max} between 0.1 and 40, α between 0.01 and 0.08, R_{10} between 0.1 and 8.0, and Q_{10} between 1.8 and 2.2. Eq. (3) was used, along with meteorological measurements (PPFD and *T*), to calculate NEE and to partition NEE between gross ecosystem photosynthesis (GEP, positive values indicate CO_2 uptake by the ecosystem) and total ecosystem respiration (TER) so that integrated growing season carbon budgets could be determined (-NEE = GEP-TER). This required information on seasonal variation in each of the equation parameters (A_{max}, α, R_{10}, Q_{10}) determined from the calculations done on two-week or monthly periods during the growing season. The 2014 and 2015 growing season C budgets were calculated by the integration of available EC measurements with gap-filled data calculated using the NEE model (Eq. (3)) when EC measurements were not available. The gap-filling and partitioning procedure used here had been tested previously, and compared well with the Fluxnet-Canada standard protocol for these analyses when using data for periods of one year or longer (Barr et al., 2004; Syed et al., 2006). For shorter time periods (4–5 months, as in this study), the NEE partitioning and gap-

filling method based on using Eq. (3) works better than protocols developed for annual and longer time periods.

An estimate of the total random uncertainty in the eddy covariance NEE measurements was obtained using the "model residual approach" of Richardson et al. (2012) by comparing the observed NEE fluxes to model calculations of NEE based on Eq. (3) for the same time periods. We used these uncertainties and the growing-season average (absolute value) NEE value to calculate relative, total random uncertainties of 22.5% and 20.5% in 2014 and 2015, respectively. We also estimated the systematic uncertainty associated with use of the friction velocity threshold screening procedure for removing data under low turbulent conditions. To do this, we repeated the gap-filling and NEE partitioning procedure described above after applying alternative friction velocity thresholds of 0.36 and 0.42 m s^{-1} (compared to our established value of 0.39 m s^{-1}). The average difference in cumulative NEE (May-August) for these alternative friction velocity thresholds was small, with only 0.44% (2014) and 0.21% (2015) change in cumulative growing season NEE calculated relative to values obtained with our established friction velocity threshold of 0.39 m s^{-1}.

2.5. Growing season water budget calculations for the HSNR

Gap-filling of missing EC data for water budget calculations was done using the Penman-Monteith equation (Monteith, 1965) to calculate ecosystem ET. All the required meteorological data were available to drive the Penman-Monteith equation, but we needed to develop a leaf phenology model and a stomatal conductance model (described below) in order to apply the full Penman-Monteith equation in our ET calculations. Our approach in developing a leaf phenology model was guided by two empirical observations. First, canopy gross photosynthesis rates in broad-leaf deciduous trees tend to decline as leaves age after the seasonal peak, even while canopy LAI measurements remain at peak values (Keenan et al., 2014). Second, there is a strong physiological link between leaf photosynthetic capacity and stomatal conductance (Wong et al., 1979). So we used our gap-filled, daily-integrated calculations of gross ecosystem photosynthesis (g C m^{-2} day^{-1}), based on eddy covariance measurements, as a proxy for describing temporal (phenological) variation in functional leaf area.

2.5.1. Leaf phenology model

A leaf phenology model, which was driven by seasonal variation in air temperature, daily total PPFD and available soil moisture, was developed and fit to seasonal variation in daily GEP in order to calculate temporal changes in functional leaf area. The leaf phenology model had the following form:

$$FunctionalLAI = f(T)f(Q)f(A_w) \quad (4)$$

where $f(T)$ is a temperature function, $f(Q)$ is a PPFD function, and $f(A_w)$ is a soil moisture function, all these functions vary between 0 and 1 with the details explained below.

$$f(T) = \left(\frac{a}{(1 + e^{-b(T_{accl} - c)})}\right) \quad (5)$$

where fitted constant a is the maximum value for $f(T)$, fitted constant b is the slope when $f(T)$ is at 50% of maximum, fitted constant c is the temperature at which $f(T)$ is 50% of maximum, and T_{accl} is the acclimation temperature (Makela et al., 2004; Kolari et al., 2007), which accounts for the lagged response of leaf development to changes in air temperature. The lagged response was based on a 200 h time constant that was previously found to work well for describing the acclimation of photosynthesis to temperature changes in different tree species (Kolari et al., 2007; Flanagan et al., 2012). The T_{accl} in the current time period ($T_{accl(i)}$) was calculated from the change in T_{accl} (ΔT_{accl}) and the T_{accl} from the previous time period ($T_{accl(i-1)}$):

$$T_{accl(i)} = \Delta T_{accl} + T_{accl(i-1)} \quad (6)$$

$$\Delta T_{accl} = \left(\frac{T_{air} - T_{accl(i-1)}}{\tau}\right) dt \quad (7)$$

where T_{air} is the measured air temperature (daily average value), dt is change in time (24 h) and τ is the lag period (200 h). The calculations were initiated with T_{accl} set equal to T_{air} on 1 April.

The $f(Q)$ was calculated from the sum of theoretical direct and diffuse solar radiation input as described by Campbell and Norman (1998, pp. 167–175) using an atmospheric transmittance of 0.75, with a value for the top of the atmosphere PPFD of 2737 μmol m^{-2} s^{-1} (400–700 nm) [which was calculated by assuming the solar constant was 1360 W m^{-2}, and that the proportion of solar radiation in the 400–700 nm region was 0.473 (Papaioannou et al., 1993), and that the average energy per mole of photons in the 400–700 nm region was 235 kJ/mol (Campbell and Norman, 1998)]. The daily-integrated values of theoretical PPFD input were calculated for all days in May-October and used to express $f(Q)$ as a relative (0–1) function by dividing by the maximum calculated daily-integrated PPFD that occurred on the summer solstice (day 172).

$$f(Aw) = \left(\frac{(Aw - 0)(Aw - Max)}{(Aw - 0)(Aw - Max) - (Aw - Opt)^2}\right) \quad (8)$$

where A_w is available soil moisture, a relative measure calculated based on the soil volumetric moisture measurements made at four depths through the soil profile and integrated vertically to calculate the total moisture content in the upper 2.5 m of soil. Available soil moisture (A_w) was specifically defined as the ratio of actual available soil water (difference between a given daily volumetric measurement and the minimum volumetric soil water content) to maximum available soil water (difference between maximum and minimum volumetric soil water contents). The maximum volumetric water content (1577 mm) was recorded during the flood conditions of June 2014 and the minimum (250 mm) value was estimated from the permanent wilting point in the soil type at our study site. *Opt* is a fitted constant, the value of A_w at which $f(A_w)$ is at its maximum (1), and *Max* is a fitted constant, the maximum value of A_w that results in the return of the $f(A_w)$ function to zero, and acts to define the shape of the $f(A_w)$ function.

The values of the five constants (*a, b, c, Opt, Max*) were determined by fitting Eq. (4)–(8) to daily relative GEP values, using the measured air temperature, calculated PPFD and measured soil moisture content for May-September in both 2014 and 2015. The daily GEP values were set to a relative scale (0–1) for each year by dividing by the seasonal maximum GEP value for that year. Our objective was to fit the leaf phenology model as a boundary line to the observed relative GEP values, with one set of model constants applied for both study years. The following values were determined for the functional leaf area model constants: $a = 1.15$, $b = 0.4$, $c = 12$, $Opt = 0.77$, $Max = 2$. Finally, the seasonal peak of measured LAI (1.8) was multiplied by the *Functional LAI* (Eq. (4)–(8)) to obtain a seasonal pattern of change in the absolute functional leaf area index (see Fig. 9).

2.5.2. Stomatal conductance model

In order to develop a model for stomatal conductance, we first produced a set of surface or canopy conductance calculations that were obtained by inverting Penman–Monteith equation (Monteith, 1965) following the approach described by Wever et al. (2002). These calculations made use of the following inputs: (i) evapo-transpiration rates measured by eddy covariance and

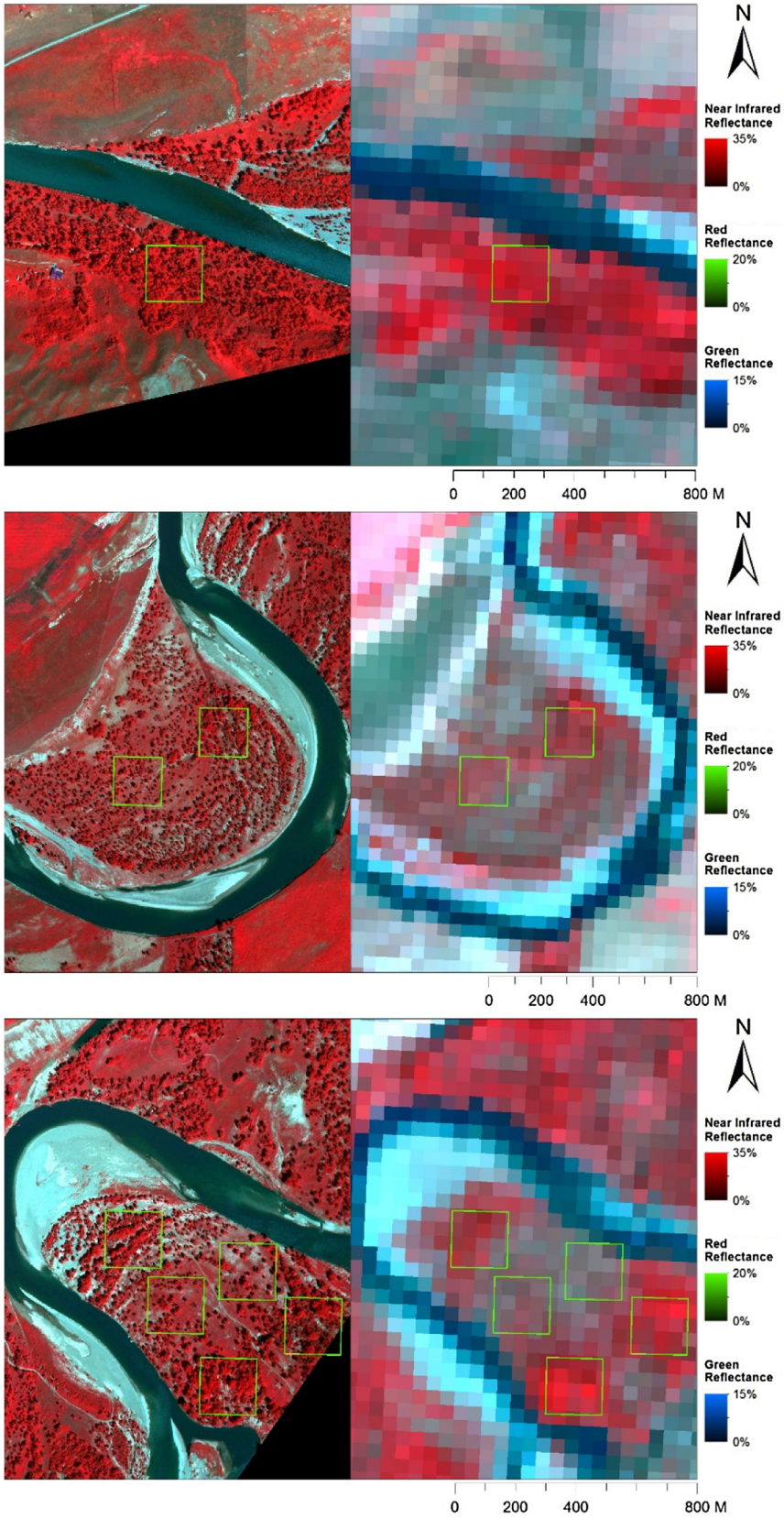

Fig. 2. Images used for riparian cottonwood forest LAI calculations along the Oldman River corridor. The three different rows represent three separate cottonwood forest sites with their locations noted in Fig. 1. Within each row, the image on the left is a digital airborne reconnaissance color infrared image with a spatial resolution of 1 m acquired around the time of peak LAI (July 29, 2014), and the image on the right is the corresponding area as imaged by Landsat 8 OLI using a similar band combination. Within a forest site the LAI study plots are indicated on both images (yellow squares, 120 m x 120 m). The digital airborne reconnaissance images allowed for careful plot selection within a forest site by providing enhanced spatial resolution compared to the satellite imagery. (For interpretation of the references to colour in this figure legend, the reader is referred to the web version of this article.)

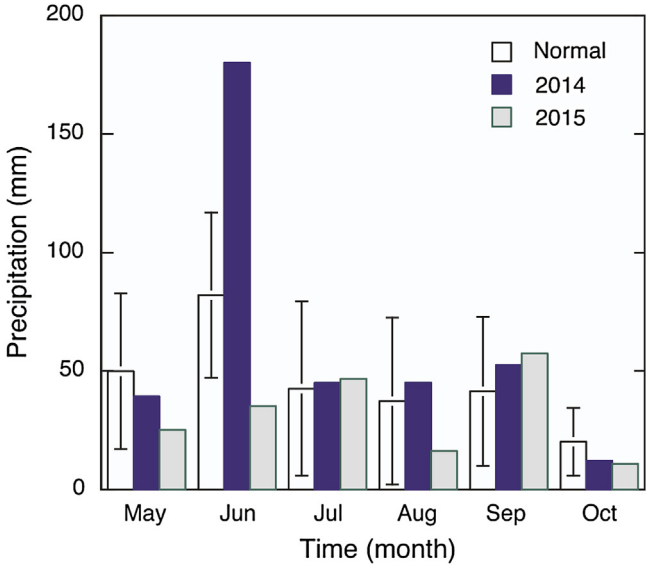

Fig. 3. Monthly total precipitation recorded in Lethbridge, Alberta during 2014 and 2015. Also shown is the climate normal precipitation (30-year average ± SD, 1981–2010).

(ii) the associated environmental conditions, that had been bin-averaged by time of day for separate monthly data (May–July) collected in both 2014 and 2015. Thus, we generated six sets of the mean diurnal pattern of canopy conductance, one for each month in 2014 and 2015. The associated mean diurnal pattern of stomatal conductance was determined by dividing the monthly canopy conductance values by the average absolute functional leaf area index values for each month (May–June) i.e. canopy conductance (mmol m^{-2} s^{-1}; ground area) = stomatal conductance (mmol m^{-2} s^{-1}; leaf area) × LAI (m^2 m^{-2}; leaf area per ground area). The combined six sets of data for the mean diurnal pattern of stomatal conductance were used to develop and parameterize a stomatal conductance model as described below.

We used a model of the form proposed by Jarvis (1976) for stomatal conductance (g, mmol m^{-2} s^{-1}):

$$g = g_{max} f(Q) f(A_w) \quad (9)$$

where g_{max} is a maximum value of stomatal conductance (mmol m^{-2} s^{-1}), $f(Q)$ and $f(A_w)$ are functions that vary between 0 and 1 and describe the response of stomatal conductance to incident photosynthetic photon flux density (Q, μmol m^{-2} s^{-1}) and available soil moisture (A_w, unit less), respectively. The g_{max} value was calculated as a function of vapor pressure deficit (D, hPa) using the equation proposed by Lloyd (1991):

$$g_{max} = \frac{1}{k_D (D)^{0.5}} \quad (10)$$

where k_D is a fitted constant. The function for response to PPFD was based on an equation used to describe electron transport (Harley et al., 1992):

$$f(Q) = \left(\frac{Q \propto}{\left[1 + \frac{Q^2 \propto^2}{g_{max}^2}\right]^{0.5}} \right) \left(\frac{1}{g_{max}} \right) \quad (11)$$

where α is a fitted constant. Eq. (8) was used for the response of stomatal conductance to available soil moisture, $f(A_w)$.

Non-linear least-squares regression was used to obtain estimates of the parameters k_D, α, *Opt* and *Max* with Matlab software, as described above. The stomatal conductance model was fit to the six monthly sets of the mean diurnal pattern of stomatal conductance and associated environmental data. The following values were calculated for the stomatal conductance model constants: $k_D = 8.61 \times 10^{-4}$, α = 0.431, *Opt* = 0.769, *Max* = 1.066.

An estimate of the total random uncertainty in the eddy covariance ET measurements was obtained using the "model residual approach" of Richardson et al. (2012) by comparing the observed ET fluxes to Penman-Montieth equation calculations of ET for the same time periods. We used these uncertainties and the growing-season average (absolute value) ET values to calculate relative, total random uncertainties of 20.0% and 4.4% in 2014 and 2015, respectively.

2.6. Ecosystem water-use efficiency

Ecosystem water-use efficiency (WUE, mmol mol^{-1}) was calculated as the ratio of gross ecosystem photosynthesis (GEP) to ecosystem ET. These daily average calculations made use of the half-hour time periods between 10:00 and 17:00 h when VPD was high, and near the daily maximum. In order to reduce the contribution of the evaporation component of ET, days with recorded precipitation were excluded. In addition, we also excluded any time periods with low ET fluxes (0.05 mmol m^{-2} s^{-1}) and inadequate turbulence ($u^* < 0.15$ m s^{-1}), as described in Ponton et al. (2006). We made WUE calculations during the period of time when the ecosystem was near peak photosynthetic activity (June–July, days 152–212).

2.7. Scaling-up cottonwood forest ET for the Oldman River corridor

Riparian cottonwood forest ET was calculated for all forest areas along the Oldman River from the Oldman River Dam to the city of Lethbridge (at the Highway 3 bridge, see Fig. 1), a total distance along the river of 171 km (referred to subsequently as the river corridor):

$$ET_{corridor} = ET_{PM} \times LAI_{corridor} \times Area_{total} \quad (12)$$

where $ET_{corridor}$ is the calculated forest ET for the entire corridor, $LAI_{corridor}$ is the area-weighted average cottonwood forest LAI along the corridor, and $Area_{total}$ is the total area of all riparian forests along the river transect. The ET calculations (ET_{PM}) were done using the Penman-Monteith equation with gap-filled meteorological input data from the HSNR study site in 2014 and 2015. The parameterized stomatal conductance model was also used to provide input data to the Penman-Monteith equation for the ET calculations. The parameterized functional leaf area model was used to determine seasonal changes in leaf area, while the absolute leaf area index of cottonwood forests ($LAI_{corridor}$) along the Oldman River corridor were determined as described below.

Using a high resolution satellite base map, riparian cottonwood forest areas were manually outlined using commercial GIS software (ArcGIS Version 10.1, ESRI, Redlands, CA, USA) and the total cottonwood forest area along the Oldman River corridor was estimated ($Area_{total}$ = 5637 ha or 56.37 km^2). The absolute peak LAI of these forests was estimated based on vegetation greenness measurements from satellite images taken along the Oldman River corridor and a local calibration curve empirically developed between vegetation greenness and LAI measured on the ground in 120 m × 120 m sample plots. To develop the local calibration curve, we first identified accessible cottonwood forest sites using high spatial resolution color infrared airborne reconnaissance imagery acquired on July 29th, 2014 (peak LAI). Three locations were selected that had substantial apparent variation in vegetation greenness within and among the sites (see Fig. 1 for forest site locations). The reconnaissance digital images had a nominal spatial resolution of 1 m and display near infrared (0.8–0.93 μm), red (0.55–0.64 μm) and green

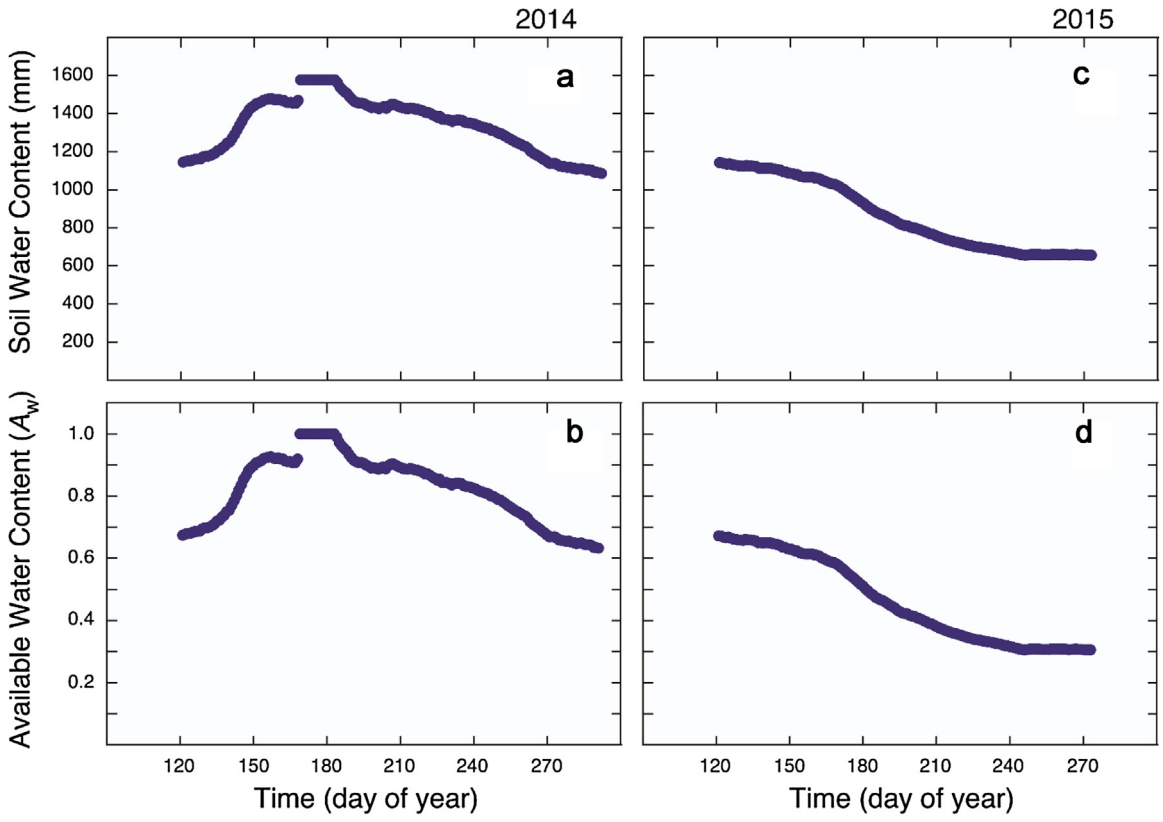

Fig. 4. Seasonal variation in daily average soil moisture content in the top 250 cm depth during (a) 2014 and (c) 2015. Available soil water content (A_w), a relative (0–1 scale) soil moisture content during (b) 2014 and (d) 2015.

(0.47–0.56 μm) reflectance as reds, greens, and blues respectively. These reconnaissance images (Fig. 2 – left side) are shown with the corresponding area as imaged by Landsat 8 OLI (Fig. 2 – right side) for the separate sites. At one forest site with high apparent greenness we established one 120 m × 120 m plot (Fig. 2 top panels), a second site had two plots, one in an area of low greenness and one in an area of moderate vegetation greenness (Fig. 2, middle panels). At the final forest site, we established 5 study plots, 2 in areas of high apparent greenness, 1 in an area of moderate greenness and 2 in areas of low apparent greenness (Fig. 2 bottom panels). Landsat 8 Operational Land Imager (OLI) image data were downloaded from the United States Geological Survey (USGS) data portal (http://earthexplorer.usgs.gov/). These Landsat 8 products were already geo-rectified, atmospherically corrected, and calibrated to spectral reflectance by the USGS. For each of the eight 120 × 120 m plots from the three separate cottonwood forests, the average normalized difference vegetation index (NDVI) was calculated from the image spectra from all 16 pixels (30 m × 30 m pixels) associated with a 120 m × 120 m plot using ENVI Version 5.1 software (Exelis VIS, Boulder, CO, USA):

$$\mathrm{NDVI} = (\mathrm{NIR} - \mathrm{Red})/(\mathrm{NIR} + \mathrm{Red}) \quad (13)$$

where NIR is the reflectance in the near infrared spectral band (wavelength: 0.85–0.88 μm) and Red is the reflectance in the red spectral band (wavelength: 0.64–0.67 μm) from the Landsat 8 imagery (see Fig. 2, right-side panels). The average NDVI value for each sample plot was compared to empirical forest LAI measurements conducted on the ground in the 8 sample plots during August 2015. The LAI-2000 and TRAC instruments were used to measure tree canopy LAI, and biomass harvest measurements were used to determine the LAI of low stature understory plants in the plots, using methods described above. The NDVI values were calculated from cloud-free Landsat 8 imagery collected as close as possible to the dates of ground LAI measurements for this exercise (±4 days). A linear regression between the ground LAI measurements and Landsat 8 NDVI produced the following local calibration curve:

$$\mathrm{LAI} = 2.2662\mathrm{NDVI} - 0.0724 (r^2 = 0.718, \mathrm{n} = 8) \quad (14)$$

An area-weighted average LAI value (LAI_{corridor}) was calculated for all the cottonwood forests along the Oldman River corridor using NDVI values calculated from a Landsat 8 OLI image acquired on July 22, 2015:

$$LAI_{corridor} = \sum_{i}^{N} LAI_i * Area_i / Area_{total} \quad (15)$$

where $\mathrm{LAI_i}$ is the LAI of riparian forest *i* determined from the empirical regression between LAI and NDVI (Eq. (14)), $\mathrm{Area_i}$ is the area of riparian forest *i*, and $\mathrm{Area_{total}}$ is the total area of all riparian forests along the river transect (56.37 $\mathrm{km^2}$). This calculation resulted in an area-weighted average LAI of 1.44 for the Oldman River corridor.

Calculations of riparian cottonwood forest ET were compared to daily average flow rates of the Oldman River as recorded at Lethbridge (water ID station 05AD007, near the highway 3 bridge), values that are archived and available at the Water Survey of Environment Canada (http://wateroffice.ec.gc.ca).

3. Results

3.1. Comparison of environmental conditions in 2014 and 2015

Precipitation inputs during all growing season (May–October) months except June were quite similar in 2014 and 2015 and also close to the long-term average (1981–2010, ±SD) for those months (Fig. 3). However, more than double the normal precipitation occurred in June 2014 (Fig. 3), and this resulted in contrasting

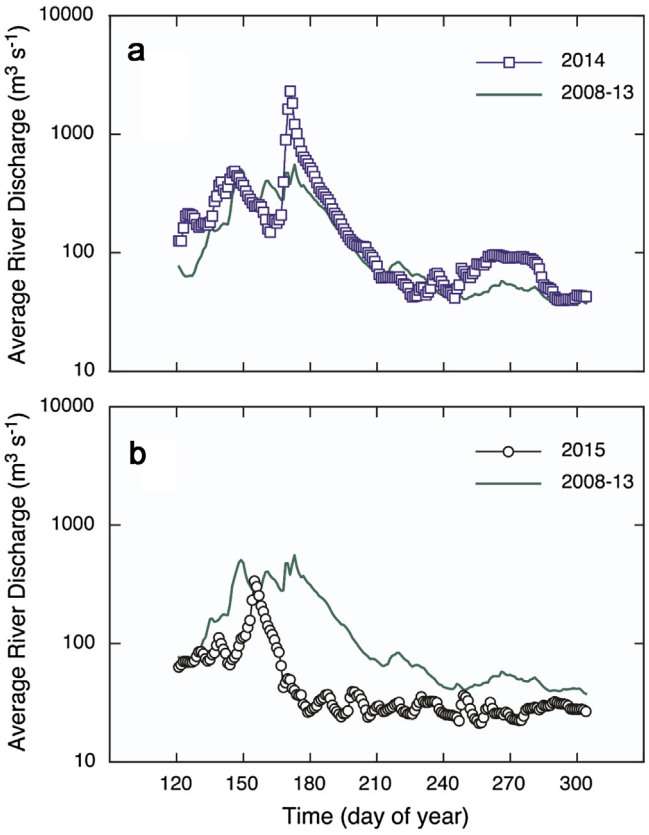

Fig. 5. Seasonal variation in daily average discharge of the Oldman River in 2014 (a) and 2015 (b) compared to average river discharge rates measured during 2008–2013 at Lethbridge, Alberta.

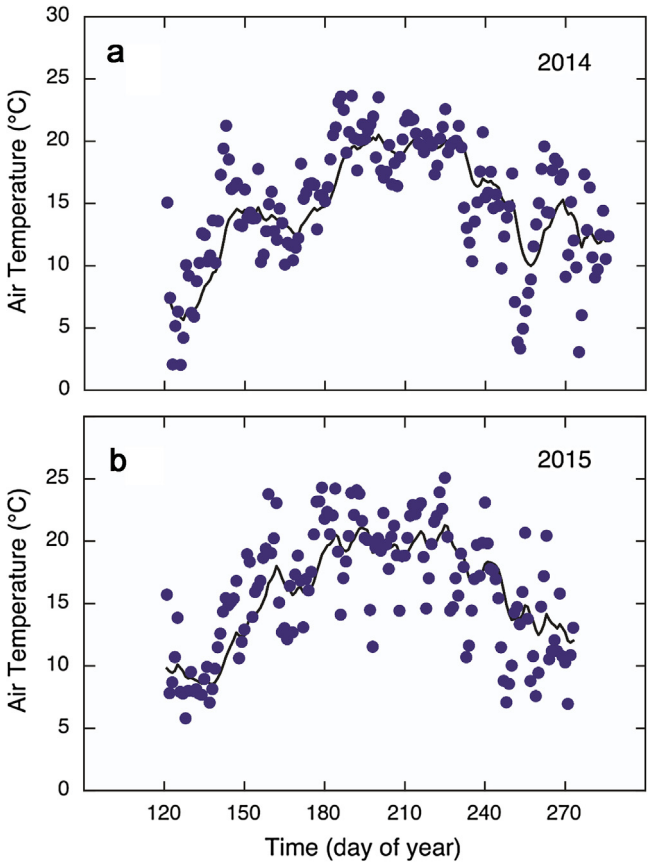

Fig. 6. Seasonal variation in the daily average air temperature (1 m) in a cottonwood forest at Helen Schuler Nature Reserve in Lethbridge, Alberta during (a) 2014 and (b) 2015. The solid black line in each figure shows the acclimation temperature (T_{accl}, Eq. (6), (7)).

seasonal patterns of soil moisture content (Fig. 4) and Oldman River discharge (Fig. 5) in 2014 and 2015, with over-bank flooding of the river apparent in June 2014. Total precipitation recorded during the entire May–October period was higher in 2014 (374 mm) than 2015 (192 mm) and the long-term average (±SD) for Lethbridge (268 ± 92 mm). The 2014 flood of the Oldman River was typical for this region in that the flood occurred during the time period from late May to early July when soils in the upper catchment of the watershed are near saturation, and it was caused by a substantial precipitation event. Floods in this region are generally not associated with annual variation in snow-pack conditions in the Oldman River watershed (Rood et al., 1998, 2007).

The seasonal pattern of daily average air temperatures was similar in the two study years, except that there were cool temperatures in June of 2014 (days 156–170) associated with the high precipitation inputs during that month, and there was a second low temperature period recorded in early September of 2014 (centered on day 253, Fig. 6).

3.2. Leaf area in the HSNR

The cottonwood tree canopy was at peak leaf area of $0.9 \pm 0.1\ m^2\ m^{-2}$ between July 11th (day 192) and August 26th (day 238) in 2014 based on the LAI-2000 and TRAC measurements. The understory LAI reached a peak of $0.9 \pm 0.2\ m^2\ m^{-2}$, so the total LAI of the HSNR was $1.8 \pm 0.2\ m^2\ m^{-2}$ with the tree canopy and understory plants contributing about equally. The tree canopy LAI calculated from leaf litter collections ($1.3 \pm 0.4\ m^2\ m^{-2}$) was similar, but slightly higher and much more variable than the tree LAI determined with the LAI-2000 and TRAC instruments.

Table 1
Comparison of non-linear regression parameters estimated using Eq. (3) for July 1–15 during 2014 and 2015. Eq. (3) was parameterized using diurnal means of net ecosystem exchange (NEE), photosynthetically-active photon flux density (PPFD) and air temperature (T), as shown in Fig. 7. r^2 is the coefficient of determination for each regression model.

	2014	2015
A_{max}	40	40
α	0.067	0.045
R_{10}	7.7	4.5
Q_{10}	1.8	1.8
r^2	0.90	0.84

3.3. Ecosystem CO_2 exchange in the HSNR

The mean diurnal patterns for NEE, PPFD and air temperature during the peak of the growing season (July 1–15) were very similar between the two study years (Fig. 7). Eq. (3) was fitted to the NEE data and allowed comparison of ecosystem photosynthetic and respiratory capacities. The calculated peak ecosystem maximum photosynthetic capacity (A_{max}) and photochemical efficiency (α) were similar in the two years, while respiratory capacity (R_{10}) was higher in 2014 than 2015 (Table 1, Fig. 7).

The seasonal pattern of daily-integrated GEP had similar initial increases in the spring and similar peak values, but GEP declined sooner and at a slightly higher rate after the July peak in 2015 than in 2014 (Fig. 8). The leaf phenology model (Eq. (4)–(8)) was fit to seasonal changes in relative GEP from both 2014 and 2015, and provided a description of seasonal changes in functional LAI (Fig. 9). The leaf phenology model showed a slightly extended growth season

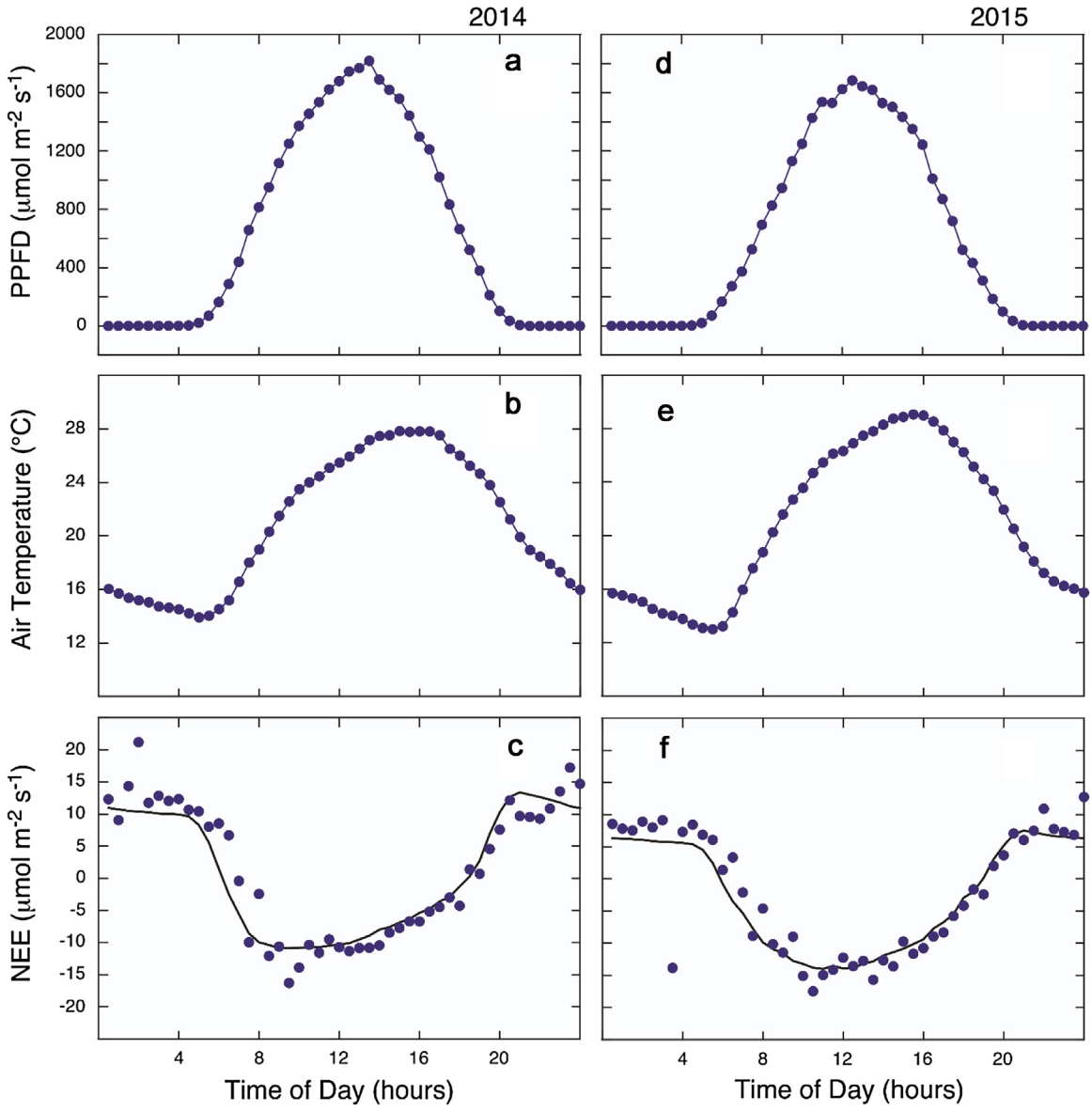

Fig. 7. Mean diurnal patterns of photosynthetically active photon flux density (PPFD) (a, d), air temperature (b, e), and net ecosystem CO_2 exchange (NEE) (c, f) in a cottonwood forest at the Helen Schuler Nature Reserve in Lethbridge, Alberta during July 1–15 in 2014 and 2015. The solid black line in component figures *c* and *f* represent Eq. (3) fitted to the measured data, which is shown as blue circles (see Table 1). (For interpretation of the references to colour in this figure legend, the reader is referred to the web version of this article.)

after the peak during 2014 compared to 2015 (Fig. 9), which was likely related to the higher soil moisture apparent in 2014 (Fig. 4).

When integrated over May-August, net ecosystem carbon uptake was greater in 2015 than 2014, the result of lower TER in 2015 while GEP values were similar in both years (Table 2). The ratio of TER and GEP was 0.94 in 2014 and 0.76 in 2015.

Table 2
Comparison of the May-August cumulative CO_2-C budget (g C m^{-2}) during 2014 and 2015 for the Helen Shuler Nature Reserve (HSNR) in Lethbridge, Alberta. NEE is net ecosystem exchange, GEP is gross ecosystem photosynthesis, and TER is total ecosystem respiration (-NEE = GEP – TER). Error bars represent total random uncertainties calculated for the eddy covariance measurements.

	2014	2015
NEE	−73 ± 16	−268 ± 55
GEP	1175 ± 264	1137 ± 233
TER	1102 ± 248	869 ± 178
TER:GEP	0.94	0.76

3.4. Ecosystem water flux at the HSNR

The mean diurnal pattern of latent heat flux in July 2014 showed higher peak values than were observed for 2015, despite similar net radiation during the two time periods (Fig. 10). As a consequence, sensible heat flux during July 2015 reached slightly higher peak values than were observed in 2014 (Fig. 10b,e). Canopy conductance values, calculated from the inversion of Penman-Monteith equation, reached higher values in July of 2014 than in 2015 (Fig. 10c,f).

The seasonal patterns and peak rates of daily-integrated ET from our gap-filled data sets were similar in both study years, although the seasonal time period for ET was slightly extended during 2014 compared to 2015 (Fig. 11a,c). Cumulative ET from May-September (±random uncertainty) was slightly higher in 2014 (451 ± 90 mm) than 2015 (411 ± 18 mm), and ET exceeded cumulative precipitation inputs in both years, although the difference between ET and precipitation was much larger in 2015 (230 mm) than in 2014 (89 mm) (Fig. 11b,d). For comparison, cumulative potential ET for

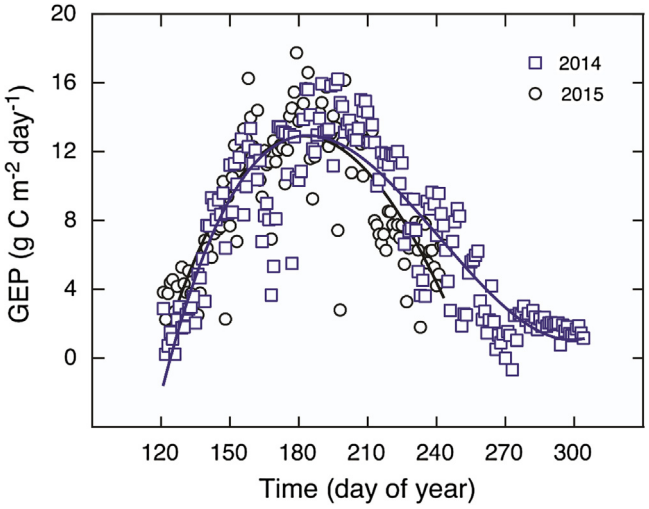

Fig. 8. Seasonal variation in the daily-integrated gross ecosystem photosynthesis (GEP) rates in a cottonwood forest at the Helen Schuler Nature Reserve in Lethbridge, Alberta during 2014 (blue squares) and 2015 (black circles). The solid lines represent polynomials fitted to the data: 2014, $1.556 \times 10^{-5} x^3 - 0.01127 x^2 + 2.566 x - 174.6$, $r^2 = 0.79$; 2015, $5.773 \times 10^{-6} x^3 - 0.006045 x^2 + 1.629 x - 118.1$, $r^2 = 0.67$. (For interpretation of the references to colour in this figure legend, the reader is referred to the web version of this article.)

May–September calculated with the Penman-Monteith equation was Monteith equation was 1583 mm in 2014 and 1922 mm in 2015.

Average (±SD) ecosystem WUE during June-July was similar in both study years (2014, 4.9 ± 1.0 mmol mol^{-1}; 2015, 4.5 ± 1.1 mmol mol^{-1}). In addition, there was a significant negative correlation between WUE and VPD in both years (2014, $r = -0.64$, n = 38, P < 0.05; 2015, $r = -0.52$, n = 59, P < 0.05). The slightly lower average WUE observed in 2015 compared with 2014, was associated with a higher average VPD (2014, 1.56 ± 0.60 kPa; 2015, 2.18 ± 0.87 kPa).

3.5. Scaling-up cottonwood forest ET for the Oldman River corridor

We calculated the daily average ET for all riparian forests along the 171 km Oldman River corridor using our area-weighted average LAI calculation of 1.44 for these forests, the Penman-Montieth equation and our parameterized stomatal conductance and leaf phenology models. The calculated rates of ET peaked at approximately 5 mm/day in July, and the cumulative forest ET during May-September for the river transect was 339 mm in both study years (Fig. 12a). Cottonwood forest ET during May and June was less than 1% of average river flow rates during 2008–2013, but the ratio of ET to average river flow rate increased markedly to maximum values of approximately 4–5% in late July and early August before declining through to the end of September in both years (Fig. 12b). Integrated over the 56.37 km^2 area of riparian cottonwood forest present along the Oldman River corridor, the cumulative forest ET during May-September was 19.1 million m^3 in both years or about 0.9% of the average (2008–2013), cumulative (May-September) Oldman River discharge (2098 million m^3).

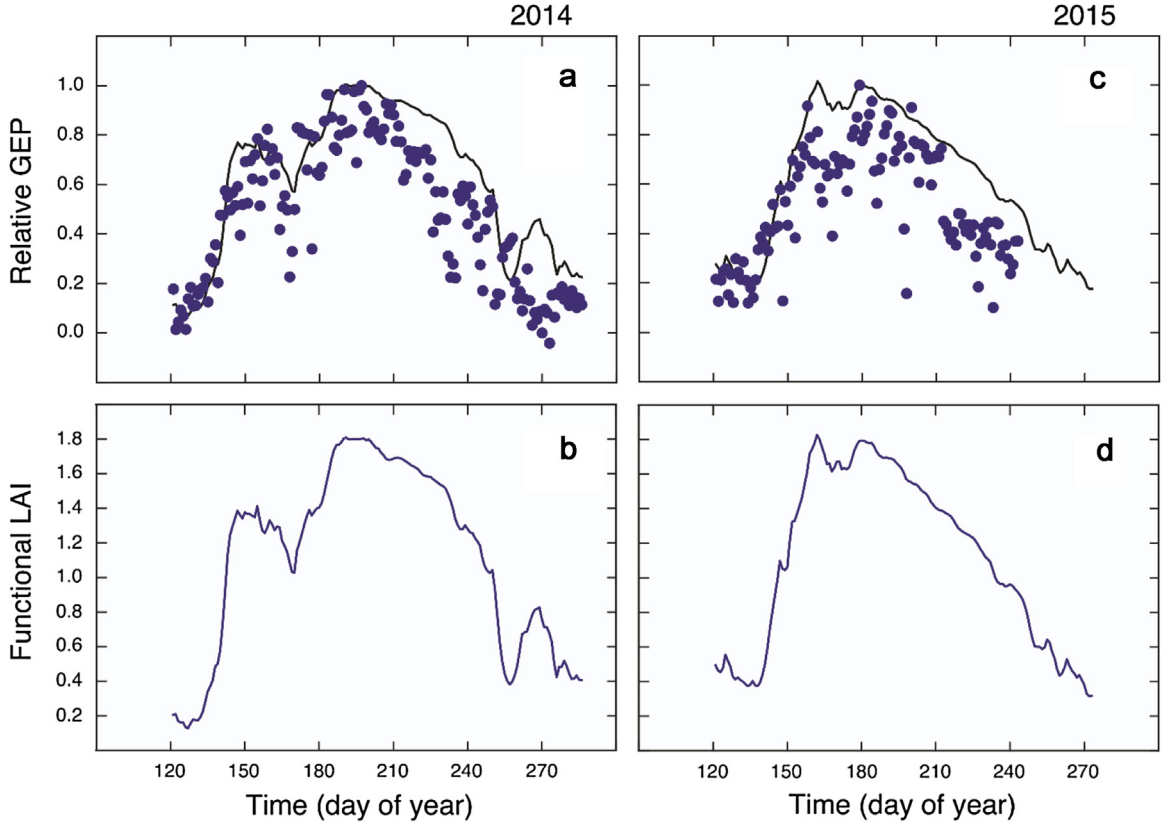

Fig. 9. Seasonal variation in relative daily gross ecosystem photosynthesis (GEP, solid blue circles) and the functional leaf area index model (black line, Eq. (4)–(8)) fitted as a boundary line to the GEP data in 2014 (a) and 2015 (c). Calculated seasonal variation in functional leaf area index (LAI) based on a measured seasonal peak LAI of 1.8 in 2014 (b) and 2015 (d). (For interpretation of the references to colour in this figure legend, the reader is referred to the web version of this article.)

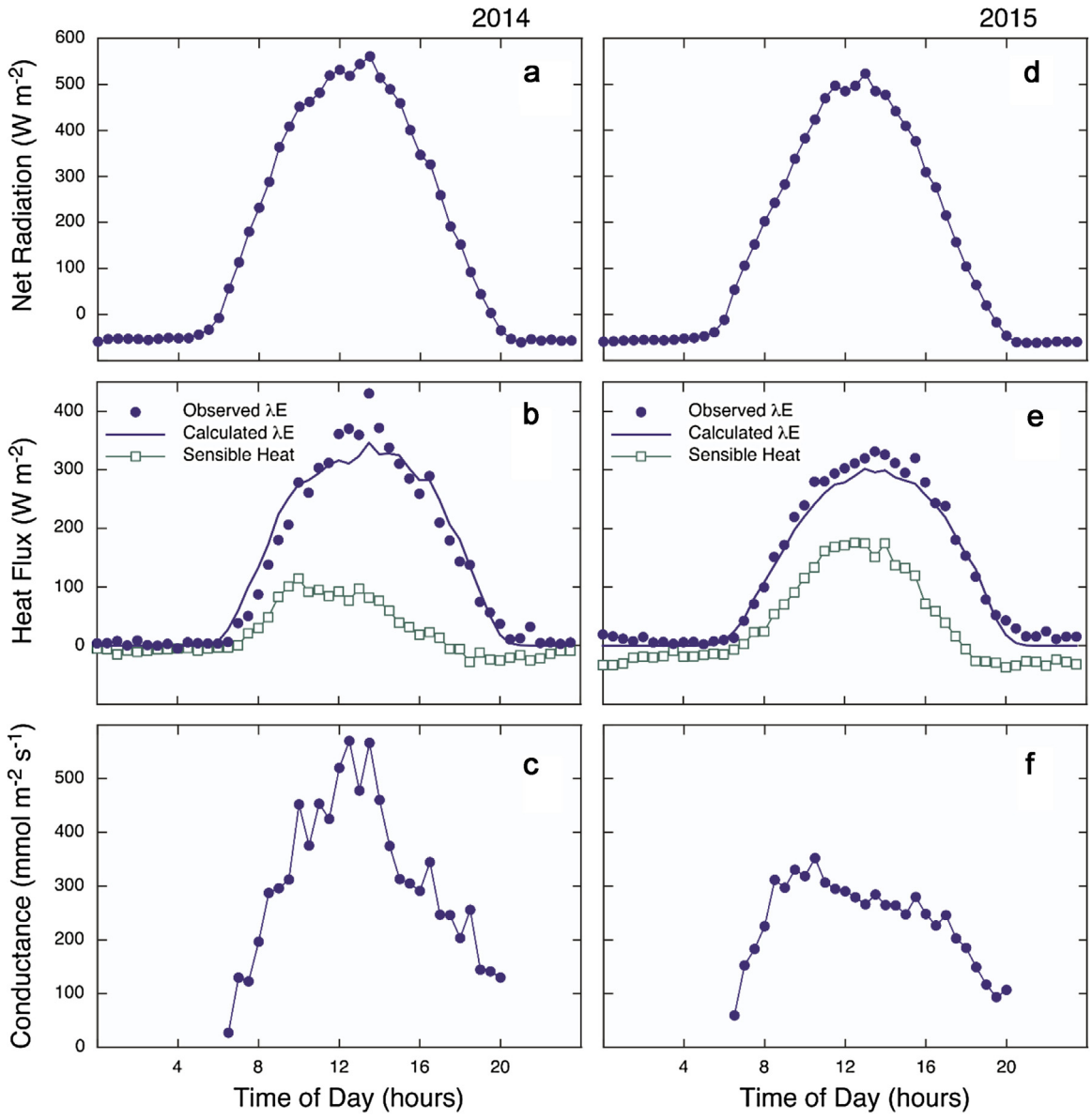

Fig. 10. Mean diurnal patterns for measured net radiation (a, d), latent heat flux (λE) and sensible heat flux (b, e), and calculated canopy conductance (c, f) during July in 2014 and 2015. The line showing "calculated latent heat flux" represents calculations done using the Penman-Montieth equation.

4. Discussion

Our measurements and calculations of riparian cottonwood forest CO_2 and H_2O exchange were influenced by a range of factors: LAI, soil moisture content, VPD, stomatal conductance and length of the growing season. Our discussion of these mechanistic controls on ecosystem gas exchange will be illustrated by using a comparative eco-physiological approach, with direct comparisons of our cottonwood riparian study site to an aspen (*Populus tremuloides*) forest on the southern edge of the boreal forest in northern Saskatchewan, and a native grassland ecosystem in southern Alberta (Ponton et al., 2006; Zha et al., 2010). The aspen forest is located just north of a vegetation (climatic) transition zone with grassland and cropland ecosystems to the south and conifer-dominated boreal forest to the north (Hogg, 1994; Hogg and Hurdle, 1995; Hogg et al., 2002, 2005). The Lethbridge grassland is representative of the dominant native vegetation in southern Alberta in areas outside of the riparian corridors (Flanagan et al., 2002; Flanagan and Atkinson, 2011). The comparison among the cottonwood, grassland and aspen sites is useful from two perspectives. First, the cottonwood and aspen are genetically-related, broad-leaf deciduous trees that are exposed to contrasting environmental conditions (temperature, VPD, precipitation, soil moisture conditions). Second, the grassland is exposed to similar aerial environmental conditions (temperature, VPD, precipitation) as the cottonwood site, albeit with contrasting soil moisture conditions, but the grassland is dominated by plants from a contrasting plant functional type (C_3 grasses) and this has significant implications for control of leaf and canopy gas exchange processes (Osmond et al., 1982; Ponton et al., 2006).

4.1. Leaf area index

The HSNR cottonwood forest and Oldman River corridor had relative low LAI (1.8 and 1.4, respectively), only approximately 50% of the Saskatchewan aspen forest (LAI averages approximately 4), but about twice that of the Lethbridge grassland during productive, wet years (Ponton et al., 2006; Zha et al., 2010). The cottonwood trees contributed about 50% of total ecosystem leaf area, similar to the

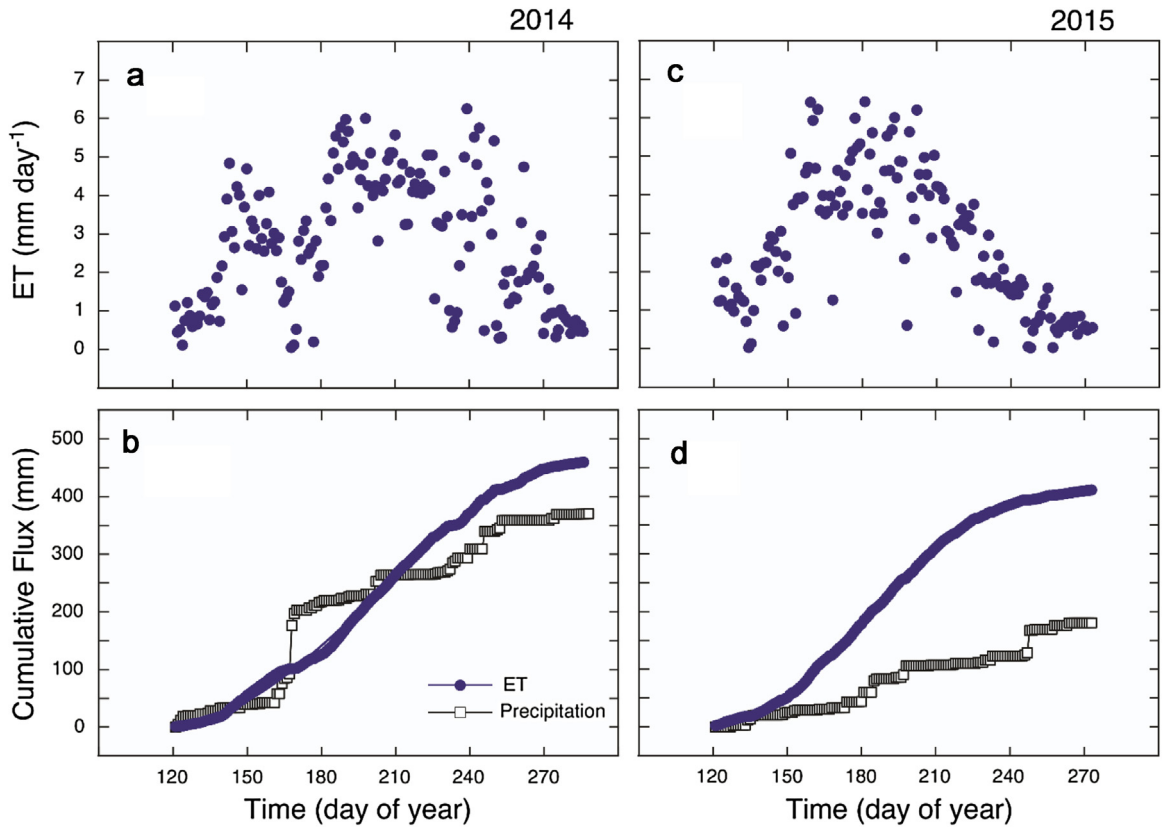

Fig. 11. Seasonal variation in the daily evapotranspiration (ET) rates in a cottonwood forest at the Helen Schuler Nature Reserve in Lethbridge, Alberta during 2014 (a) and 2015 (b); and cumulative evapotranspiration (solid blue circles) and precipitation (open black squares) fluxes in 2014 (b) and 2015 (d). (For interpretation of the references to colour in this figure legend, the reader is referred to the web version of this article.)

case for the aspen forest, where the aspen understory was dominated by a broad-leaf deciduous shrub (hazelnut, *Corylus cornuta*) (Barr et al., 2004).

4.2. Soil moisture content

Soil moisture content varied significantly within and between the two study seasons, associated with the over-bank river flooding in 2014 and the low precipitation of 2015 (Figs. 3 and 4). There was a relatively large difference between the highest and lowest integrated soil moisture content within both growing seasons (439 mm in 2014, 486 mm in 2015; Fig. 4). In addition, integrated soil moisture content was quite low during July-September 2015 (Fig. 4). However, the cottonwood forest soil also had a relatively large water storage capacity (field capacity – wilting point, 1577 – 250 = 1327 mm) compared to the shallow Lethbridge grassland soil (420 – 160 = 260 mm; Hufkens et al., 2016). In addition, the riparian cottonwood trees have roots that extend deep enough in the soil (approximately 2.5 m) to reach the capillary fringe, even when the water table is near its maximum depth below the floodplain soil surface (Rood et al., 2011, 2013). The deep-rooted cottonwood trees should be able to access groundwater (which extends almost horizontally from the river water) for much of their transpiration requirements in years with river flow rates like that observed in 2015 (Rood et al., 2013). Despite this, it has been observed that cottonwood growth rates and carbon isotope discrimination declined during years with very low river flow rates, especially in trees that were higher in elevation relative to the river or more distant from the river's bank, implying soil drought effects can affect leaf gas photosynthetic exchange (Rood et al., 2013). In addition, the more shallowly rooted herbaceous plants and small shrubs in the cottonwood forest understory are likely even more negatively influenced by the decline in soil moisture that was observed in the cottonwood ecosystem during 2015 (see below).

4.3. Ecosystem CO_2 exchange

While the cottonwood forest had similar maximum daily GEP rates in July during both study years, the reduction in GEP after the July peak occurred earlier in 2015 than in 2014 (Fig. 6), likely associated with the lower soil water content in 2015 (Fig. 4). In addition, ecosystem respiration rates were higher in 2014 than 2015 (Fig. 7, Tables 1 and 2), perhaps because the higher water content in the shallow soil layers in 2014 increased respiration of roots and microbes compared to 2015, when lower soil moisture in the shallow soil layers due to low precipitation and lack of river flooding would have likely restricted respiratory activity (Flanagan and Johnson, 2005). It is also possible that the over-bank flooding of 2014 stressed plants (Kreuzwieser and Rennenberg, 2014), and respiration increased after the flood waters retreated as physiological processes and growth recovered from the stress. Overall the difference in photosynthetic activity between the two study years was remarkably small (Table 2), given the significant contrast that was observed for precipitation and soil moisture content in 2014 and 2015 (Figs. 3 and 4).

4.4. Leaf phenology model

Our addition of a leaf phenology model to canopy conductance calculations provided a simple mechanism to account for seasonal (growing season) changes in functional LAI that have previously

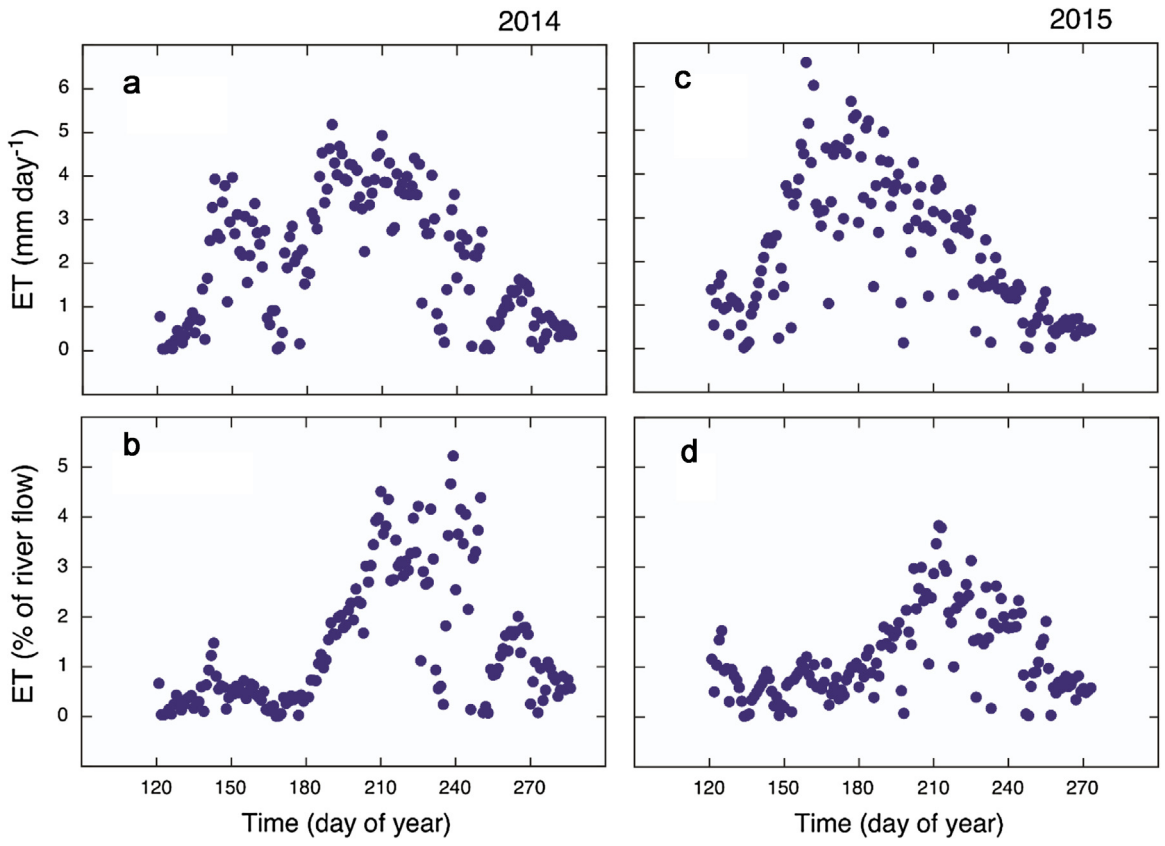

Fig. 12. Seasonal variation in the daily evapotranspiration (ET) rates in cottonwood forests along the Oldman River corridor (Oldman Dam to Lethbridge) in southern Alberta during 2014 (a) and 2015 (b); and ratio of the daily evapotranspiration flux of cottonwood forests along the transect and daily average river discharge (2008–2013) measured at Lethbridge in 2014 (b) and 2015 (d).

been noted as important for accurate ET calculations (e.g. Kasurinen et al., 2014). The leaf phenology model that we developed and applied, which included an interacting combination of temperature, radiation and soil moisture controls, was similar to that used in other phenology studies (Stockli et al., 2011). As applied in this study, the phenology model allowed explicit consideration of significant seasonal changes to leaf photosynthetic gas exchange capacity that typically occur in broad-leaf deciduous trees, even when peak canopy LAI shows limited variation within the growing season (Keenan et al., 2014). In this sense our model improves upon the phenology model applied by Kasurinen et al. (2014) to ET calculations, as the Kasurinen et al. (2014) model quickly increases to the maximum value and remains constant during the growing season months in boreal environments. Our leaf phenology model allowed a single set of parameters to be used in the stomatal conductance model for calculations across a large range of environmental conditions within and between study years.

4.5. Ecosystem H_2O exchange

Maximum values of calculated canopy conductance in the cottonwood forest (Fig. 10) were very similar to those determined for aspen forest (Blanken and Black, 2004), despite the lower LAI for the cottonwood forest. Canopy conductance includes contributions from the tree canopy, understory plants and soil evaporation. During early July 2014 there were still pools of standing water evident in the understory of the cottonwood forest, remnants from the over-bank flooding of the Oldman River in June 2014. So the relatively high canopy conductance observed for the cottonwood forest in July 2014, compared to values calculated for July 2015 (Fig. 10) and the aspen forest, may partly be related to contributions of soil evaporation to total ecosystem ET. The lower precipitation and soil moisture recorded in the cottonwood site during 2015 (Figs. 3 and 4), may have also slightly inhibited physiological activity of shallowly rooted understory plants (particularly herbaceous species) and reduced their contribution to ecosystem ET and calculated canopy conductance in July 2015.

The maximum daily ET (approximately 6 mm/day) and the cumulative total ET for the May-September growing season (± random uncertainty) in the cottonwood forest (2014: 451 ± 90 mm; 2015: 411 ± 18 mm, Fig. 11) were both higher than respective growing season values observed in the Lethbridge grassland (4–5 mm/day; 320 ± 89 mm, average ± SD, n = 8 years, Flanagan and Atkinson, 2011) and in the aspen forest (3–4 mm/day; 232 ± 43 mm, average ± SD, n = 4 years, Kljun et al., 2006). The native C_3 grass plants of the Lethbridge grassland tend to have relatively high leaf and canopy conductance rates, which in combination with the high VPD of their habitat, results in large ET rates, despite the relatively low LAI apparent in this ecosystem (Wever et al., 2002; Ponton et al., 2006). This is consistent with a strategy of grass plants to grow fast while moisture conditions are favorable and then enter dormancy during harsh, dry conditions. In contrast, the aspen forest had similar canopy conductance despite higher LAI than our cottonwood forest site (Blanken and Black, 2004), but lower ET rates because of generally cooler air temperatures, lower VPD and slightly shorter growing season than the cottonwood forest (Ponton et al., 2006). This illustrates the interaction between the biological and environmental characteristics influencing ecosystem-level water fluxes.

The cottonwood trees likely had access to alluvial groundwater that was recharged with river water and so ecosystem ET was relatively insensitive to differences in precipitation between the

two study years. During 2015, the year with low precipitation and no river flooding, cumulative ET was substantially higher than the cumulative precipitation (230 mm, Fig. 11d), consistent with the cottonwood trees accessing to groundwater/river water to support ET (Scott et al., 2003, 2004). The difference between ET and precipitation was much lower in 2014 (89 mm; Fig. 11b) because of the very high precipitation inputs in June 2014 (Fig. 4). The relatively small difference in cumulative ET between the two years (451 mm in 2014; 411 mm in 2015; Fig. 11b, d) was likely indicative that soil water availability was not limiting ecosystem ET to any major extent in either 2014 or 2015, despite the possible reduced contribution of shallow-rooted understory plants to ecosystem ET in 2015. The slightly cooler and lower VPD conditions would have also limited ET somewhat in 2014, and helped to minimize inter-annual differences in cumulative ET, even though soil moisture was higher in 2014 than in 2015 (Fig. 4). In contrast, cumulative ET followed cumulative precipitation quite closely in most years at the Lethbridge grassland site (Wever et al., 2002), as the soil water storage capacity is low at the grassland and there is no saturated groundwater table that is accessible to the plants at this site (Flanagan and Atkinson, 2011). Soil water storage in the aspen site can also help to maintain some consistency in ET among different growing seasons, as aspen trees can draw on deep soil water reservoirs causing a decline in the soil water table during years with lower precipitation, while the saturated water table recovers in years when precipitation inputs are higher than ET (Kljun et al., 2006; Zha et al., 2010). However, the ability of deep soil water to buffer variation in precipitation inputs is limited at the aspen site, and moderate soil water limitations on ET and ecosystem CO_2 exchange have been recorded at this site (Kljun et al., 2006), so in terms of groundwater access it is an intermediate case relative to the grassland and cottonwood sites.

Average cottonwood ecosystem WUE was very similar in both study years (4.5 and 4.9 mmol mol^{-1}) and close to values observed in the aspen forest (4.5–5.4 mmol mol^{-1}; Arain et al., 2002; Ponton et al., 2006). The negative relationship between WUE and VPD, that was apparent for the cottonwood forest, was also observed for the aspen forest by Ponton et al. (2006). Much lower ecosystem WUE values were observed for the Lethbridge grassland (2.6–3.1 mmol mol^{-1}; Wever et al., 2002; Ponton et al., 2006). The difference in WUE apparent between ecosystems dominated by C_3 grasses and broad-leaf deciduous trees was expected based on the known variation in leaf physiological traits between these two plant functional types (Osmond et al., 1982).

4.6. Landscape-level calculations of ET along the Oldman River corridor

We calculated that total ET of the riparian forests along the Oldman River corridor was 19.1 million m^3 at a rate of 339 mm/season during May-September. This is the same order of magnitude as estimates of total ET from riparian cottonwood-mesquite woodland of 27–36 million m^3 per year along the San Pedro River in southern Arizona (a 100 km length of river with riparian vegetation covering an area of 4500 ha with an average LAI of approximately 1.5–similar but slightly smaller characteristics than our Oldman River study system) (Scott et al., 2004; Nagler et al., 2005). However, annual ET rates in the riparian woodlands along the San Pedro River were higher (852 mm/year) than we measured for the Oldman River, but the growing season is much longer and air temperature and vapor pressure deficit are both much higher in the Arizona study area (Scott et al., 2004). A relatively large increase riparian ecosystem ET relative to Oldman River flow (2008–2013) occurred in August (Fig. 12), a time period with high air temperatures (Fig. 6) and VPD, and this illustrates the importance of maintaining sufficient river flow rates during this time in order to supply sufficient alluvial groundwater recharge into the cottonwood soil system to support the ecosystem's water use (Rood et al., 2003a, 2008).

4.7. Conclusions

Our comparative analysis showed that the water-use rates of riparian cottonwood forests are high, even for a broad-leaf deciduous forest functional type. This was particularly true given the relatively modest LAI (1.4) we measured for the cottonwood sites across the Oldman River corridor. The high ET rates we measured were caused by the relatively warm summer temperatures and high VPD, along with the lack of significant soil moisture limitation to the cottonwood tree conductance and transpiration because of sufficient access to alluvial groundwater. The cottonwood ecosystem also had very similar patterns of CO_2 and H_2O exchange (Figs. 7, 8 and 11) in two years of contrasting precipitation input and soil water content (Figs. 3 and 4). This suggested that the cottonwood trees dominated ecosystem gas exchange processes, even more than would be expected by their 50% contribution to total ecosystem LAI. The earlier reduction in GEP after the seasonal peak during 2015 compared to 2014 (Fig. 8), was likely associated with reduced activity in the shallow-rooted understory vegetation, which was probably not supplied with alluvial groundwater. Our ecosystem flux measurements were consistent with the Sperry and Love (2015) prediction that riparian cottonwood forests would be less sensitive to summer drought caused by low precipitation inputs than exposure to restricted alluvial groundwater access which is dependent on river discharge rates. We also showed that the cottonwood forest water use increased markedly relative to the Oldman River flow rates in August (Fig. 12), a time of warm temperature and high VPD (Rood et al., 2003a, 2008). Recent empirical data indicated that annual river discharge rates have declined in the South Saskatchewan River basin that includes the Oldman River, with this largely caused by an earlier onset of snowmelt resulting in low mid- to late-summer river flows (Rood et al., 2008; St-Jacques et al., 2010). Model predictions indicate a high probability of generally low river flows and extreme low flows in this basin in the future due to climate change (Shepherd et al., 2010; St-Jacques et al., 2013). This poses a significant threat to supporting the high water use requirements of cottonwood riparian forests along the Oldman River in the future. The research described here contributes directly to understanding how much water needs to remain in southern Alberta rivers to sustain healthy riparian cottonwood ecosystems.

Acknowledgements

This research was part of the *Functional Flows: A Practical Strategy for Healthy Rivers* project and was supported by grants from Alberta Innovates – Energy and Environment Solutions, the Natural Sciences and Engineering Research Council of Canada – Discovery Grant Program, and Conoco Phillips Canada. We thank Eric Sharp, Emily Wilton, Kayla Johnson, Caitlin Pelletier, Tyler Tremel, and David Pearce for help with some of the field and lab work, and Rachhpal Jassal for helpful comments on the manuscript. David Ellis (City of Lethbridge) and Coreen Putman (Helen Schuler Nature Centre, Lethbridge) provided permission to conduct research in the HSNR. We thank Mr. J. Jacobson (site 1), Mr. Kreft (Kreft Cattle Ltd, sites 4-8), and Mr. Smit (Smit Brothers Farms, sites 2 & 3) for permission to conduct leaf area sampling on their property.

References

Arain, M.A., Black, T.A., Barr, A.G., et al., 2002. Effects of seasonal and interannual climate variability on net ecosystem productivity of boreal deciduous and coniferous forests. Can. J. For. Res. 32, 878–891.

Aubinet, M., Feiger Winter, C., Heinesch, B., Laffineur, Q., Papale, D., Reichstein, M., Rinne, J., Van Gorsel, E., 2012. Nighttime flux correction. In: Aubinet, M.,

Papale, D., Vesala, T. (Eds.), Eddy Covariance: A Practical Guide to Measurement and Data Analysis. Springer, Berlin, Germany.
Baldocchi, D.D., 2014. Measuring fluxes of trace gases and energy between ecosystems and the atmosphere – state and future of the eddy covariance method. Global Change Biol. 20, 3600–3609.
Barr, A.G., Black, T.A., Hogg, E.H., et al., 2004. Inter-annual variability in the leaf area index of a boreal aspen-hazelnut forest in relation to net ecosystem production. Agric. For. Meteorol. 126, 237–255.
Blanken, P.D., Black, T.A., 2004. The canopy conductance of a boreal aspen forest, Prince Albert National Park, Canada. Hydrol. Processes 18, 1561–1578.
Campbell, G.S., Norman, J.M., 1998. An Introduction to Environmental Biophysics, 2nd ed. Springer-Verlag, New York, USA.
Chen, J.M., Govind, A., Sonnentag, O., Zhang, Y., Barr, A., Amiro, B., 2006. Leaf area index measurements at Fluxnet-Canada forest sites. Agric. For. Meteorol. 140, 257–268.
Doody, T.M., Colloff, M.J., Davies, M., Koul, V., Benyon, R.G., Nagler, P.M., 2015. Quantifying water requirements of riparian river red gum (*Eucalyptus camaldulensis*) in the Murray-Darling Basin, Australia – implications for the management of environmental flows. Ecohydrology 8, 1471–1487.
Flanagan, L.B., Atkinson, A.C., 2011. Interacting controls on productivity in a northern Great Plains grassland and implications for response to ENSO events. Global Change Biol. 17, 3293–3311.
Flanagan, L.B., Johnson, B.G., 2005. Interacting effects of temperature soil moisture, and plant biomass production on ecosystem respiration in a northern temperate grassland. Agric. Fore. Meteorol. 130, 237–253.
Flanagan, L.B., Wever, L.A., Carlson, P.J., 2002. Seasonal and interannual variation in carbon dioxide exchange and carbon balance in a northern temperate grassland. Global Change Biol. 8, 599–615.
Flanagan, L.B., Cai, T., Black, T.A., Barr, A.G., McCaughey, J.H., Margolis, H.A., 2012. Measuring and modeling ecosystem photosynthesis and the carbon isotope composition of ecosystem-respired CO_2 in three boreal coniferous forests. Agric. For. Meteorol. 153, 165–176.
Gom, L.A., Rood, S.B., 1999. Patterns of clonal occurrence in a mature cottonwood grove along the Oldman River, Alberta. Can. J. Bot. 77, 1095–1105.
Harley, P.C., Thomas, R.B., Reynolds, J.F., Strain, B.R., 1992. Modelling photosynthesis of cotton grown in elevated CO_2. Plant Cell Environ. 15, 271–282.
Hogg, E.H., Hurdle, P.A., 1995. The aspen parkland in western Canada: a dry-climate analogue for the future boreal forest? Water Air Soil Pollut. 82, 391–400.
Hogg, E.H., Brandt, J.P., Kochtubajda, B., 2002. Growth and dieback of aspen forests in northwestern Alberta, Canada, in relation to climate and insects. Can. J. For. Res. 32, 823–832.
Hogg, E.H., Brandt, J.P., Kochtubajda, B., 2005. Factors affecting the interannual variation in growth of western Canadian aspen forests during 1951–2000. Can. J. For. Res. 35, 610–622.
Hogg, E.H., 1994. Climate and the southern limit of the western Canadian boreal forest. Can. J. For. Res. 24, 1835–1845.
Hufkens, K., Keenan, T.F., Flanagan, L.B., Scott, R.L., Bernacchi, C.J., Joo, E., Brunsell, N.A., Verfaillie, J., Richardson, A.D., 2016. Productivity of North American grasslands is increased under future climate scenarios despite rising aridity. Nat. Clim. Change 6, 710–714.
Jarvis, P.G., 1976. The interpretation of the variations in leaf water potential and stomatal conductance found in canopies in the field. Philos. Trans. R. Soc. Lond. B: Biol. Sci. 273, 593–610.
Kasurinen, V., Alfredsen, K., Kolari, P., et al., 2014. Latent heat exchange in the boreal and arctic biomes. Global Change Biol. 20, 3439–3456.
Keenan, T.F., Darby, B., Felts, E., Sonnentag, O., Friedl, M.A., Hufkens, K., O'Keefe, J., Klosterman, S., Munger, J.W., Toomey, M., Richardson, A.D., 2014. Tracking forest phenology and seasonal physiology using digital repeat photography. Ecol. Appl. 24, 1478–1489.
Kljun, N., Calanca, P., Rotach, M.W., Schmid, H.P., 2004. A simple parameterisation for flux footprint predictions. Boundary-Layer Meteorol. 112, 503–523.
Kljun, N., Black, T.A., Griffis, T.J., Barr, A.G., Gaumont-Guay, D., Morgenstern, K., McCaughey, J.H., Nesic, Z., 2006. Response of net ecosystem productivity of three boreal forest stands to drought. Ecosystems 9, 1128–1144.
Kolari, P., Lappalainen, H.K., Hanninen, H., Hari, P., 2007. Relationship between temperature and the seasonal course of photosynthesis in Scots pine at northern timberline and in southern boreal zone. Tellus 59B, 542–552.
Kreuzwieser, J., Rennenberg, H., 2014. Molecular and physiological responses of trees to waterlogging stress. Plant Cell Environ. 37, 2245–2259.
Leblanc, S.G., Chen, J.M., 2001. A practical scheme for correcting multiple scattering effects on optical LAI measurements. Agric. For. Meteorol. 110, 125–139.
Leblanc, S.G., Chen, J.M., Kwong, M., 2002. Tracing radiation and architecture of canopies TRAC MANUAL version 2.1.3. Can. Centre Remote Sens.
Lloyd, J., 1991. Modelling stomatal responses in *Macadamia integrifolia*. Aust. J. Plant Physiol. 18, 649–660.
Makela, A., Hari, P., Berninger, F., Hanninen, H., Nikinmaa, E., 2004. Acclimation of photosynthetic capacity in Scots pine to the annual cycle of temperature. Tree Physiol. 24, 369–376.
Monteith, J.L., 1965. Evaporation and environment. The state and movement of water in living organisms. Symposium of the Society of Experimental Biology, vol. 19. Cambridge University Press, Cambridge, U.K, pp. 205–234.
Nagler, P.L., Scott, R.L., Westenburg, C., Cleverly, J.R., Glenn, E.P., Huete, A.R., 2005. Evapotranspiration on western U.S. rivers estimated using the Enhanced Vegetation Index from MODIS and data from eddy covariance and Bowen ratio towers. Remote Sen. Environ. 97, 337–351.
Naiman, R.J., Décamps, H., McClain, M.E., 2005. Riparia: Ecology, Conservation, and Management of Streamside Communities. Elsevier Amsterdam, The Netherlands.
Oki, T., Hanae, S., 2006. Global hydrological cycles and world water resources. Science 313, 1068–1072.
Osmond, C.B., Winter, K., Ziegler, Z., 1982. Functional significance of different pathways of CO_2 fixation in photosynthesis. In: Person, A., Zimmerman, H. (Eds.), Encyclopedia of Plant Physiology, vol. 12 B. Springer-Verlag, New York, pp. 479–547.
Papaioannou, G., Papanikolaou, N., Retalis, D., 1993. Relationships of photosynthetically active radiation and shortwave irradiance. Theor. Appl. Climatol. 48, 23–27.
Poff, N.L., Allan, J.D., Bain, M.B., Karr, J.R., Prestegaard, K.L., Richter, B.D., Sparks, R.E., Stromberg, J.C., 1997. The natural flow regime. BioScience 47, 769–784.
Ponton, S., Flanagan, L.B., Alstad, K.P., Johnson, B.K., Morgenstern, K., Kljun, N., Black, T.A., Barr, A.G., 2006. Comparison of ecosystem water-use efficiency among Douglas-fir forest, aspen forest and grassland using eddy covariance and carbon isotope techniques. Global Change Biol. 12, 294–310.
Richardson, A.D., Aubinet, M., Barr, A.G., Hollinger, D.Y., Ibrom, A., Lasslop, G., Reichstein, M., 2012. Uncertainty quantification. In: Aubinet, M., Papale, D., Vesala, T. (Eds.), Eddy Covariance: a Practical Guide to Measurement and Data Analysis. Springer, Berlin, Germany.
Richter, B.D., Richter, H.E., 2000. Prescribing flood regimes to sustain riparian ecosystems along meandering rivers. Conserv. Biol. 14, 1467–1478.
Rood, S.B., Mahoney, J.M., Reid, D.E., Zilm, L., 1995. Instream flows and the decline of riparian cottonwoods along the St. Mary River, Alberta. Can. J. Bot. 73, 1250–1260.
Rood, S.B., Kalischuk, A.R., Mahoney, J.M., 1998. Initial cottonwood seedling recruitment following the flood of the century of the Oldman River Alberta, Canada. Wetlands 18, 557–570.
Rood, S.B., Braatne, J.H., Hughes, F.M.R., 2003a. Ecophysiology of riparian cottonwoods: streamflow dependency: water relations and restoration. Tree Physiol. 23, 1113–1124.
Rood, S.B., Gourley, C., Ammon, E.M., Heki, L.G., Klotz, J.R., Morrison, M.L., Mosley, D., Scoppettone, G.G., Swanson, S., Wagner, P.L., 2003b. Flows for floodplain forests: a successful riparian restoration. BioScience 53, 647–656.
Rood, S.B., Samuelson, G.M., Braatne, J.H., Gourley, C.R., Hughes, F.M.R., Mahoney, J.M., 2005. Managing rivers to restore floodplain forests. Front. Ecol. Environ. 3, 193–201.
Rood, S.B., Goater, L.A., Mahoney, J.M., Pearce, C.M., Smith, D.G., 2007. Floods fire, and ice: disturbance ecology of riparian cottonwoods. Can. J. Bot. 85, 1019–1032.
Rood, S.B., Pan, J., Gill, K.M., Franks, C.G., Samuelson, G.M., Shepherd, A., 2008. Declining summer flows of Rocky Mountain rivers: historic hydrology and probable impacts on floodplain forests. J. Hydrol. 349, 397–410.
Rood, S.B., Bigelow, S.G., Hall, A.A., 2011. Root architecture of riparian trees: river cut-banks provide natural hydraulic excavation: revealing that cottonwoods are facultative phreatophytes. Trees 25, 907–917.
Rood, S.B., Ball, D.J., Gill, K.M., Kaluthota, S., Letts, M.G., Pearce, D.W., 2013. Hydrologic linkages between a climate oscillation, river flows, growth, and wood $\Delta^{13}C$ of male and female cottonwood trees. Plant Cell Environ. 36, 984–993.
Sauchyn, D.J., St-Jacques, J.M., Barrow, E., Nemeth, M.W., Macdonald, R.J., Sheer, A.M.S., Sheer, D.P., 2016. Adaptive water resource planning in the South Saskatchewan River Basin: use of scenarios of hydroclimatic variability and extremes. J. Am. Water Resour. Assoc. 52, 222–240.
Schindler, D.W., Donahue, W.F., 2006. An impending water crisis in Canada's western prairie provinces. Proc. Natl. Acad. Sci. USA 103, 7210–7216.
Scott, M.L., Auble, G.T., Friedman, J.M., 1997. Flood dependency of cottonwood establishment along the Missouri River, Montana, USA. Ecol. Appl. 7, 677–690.
Scott, M.L., Shafroth, P.B., Auble, G.T., 1999. Responses of riparian cottonwoods to alluvial water table declines. Environ. Manage. 23, 347–358.
Scott, R.L., Shuttleworth, W.J., Goodrich, D.C., Maddock, T., 2000. The water use of two dominant vegetation communities in a semiarid riparian ecosystem. Agric. For. Meteorol. 105, 241–256.
Scott, R.L., Watts, C., Payan, J.G., Edwards, E., Goodrich, D.C., Williams, D., Shuttleworth, W.J., 2003. The understory and overstory partitioning of energy and water fluxes in an open canopy: semiarid woodland. Agric. For. Meteorol. 114, 127–139.
Scott, R.L., Edwards, E.A., Shuttleworth, W.J., Huxman, T.E., Watts, C., Goodrich, D.C., 2004. Interannual and seasonal variation in fluxes of water and carbon dioxide from a riparian woodland ecosystem. Agric. For. Meteorol. 122, 65–84.
Serbin, S.P., Ahl, D.E., Gower, S.T., 2013. Spatial and temporal validation of the MODIS LAI and FPAR products across a boreal forest wildfire chronosequence. Remote Sens. Environ. 133, 71–84.
Shepherd, A., Gill, K.M., Rood, S.B., 2010. Climate change and future flows of Rocky Mountain rivers: converging forecasts from empirical trend projection and downscaled global circulation modeling. Hydrol. Processes 24, 3864–3877.
Sperry, J.S., Love, D.M., 2015. What plant hydraulics can tell us about responses to climate change droughts. New Phytol. 207, 14–27.
St-Jacques, J.M., Sauchyn, D.J., Zhao, Y., 2010. Northern Rocky Mountain streamflow records: global warming trends, human impacts or natural variability? Geophys. Res. Lett. 37, L06407, http://dx.doi.org/10.1029/2009GL042045.
St-Jacques, J.M., Lapp, S.L., Zhao, Y., Barrow, E.M., Sauchyn, D.J., 2013. Twenty-first century central Rocky Mountain river discharge scenarios under greenhouse forcing. Quat. Int. 310, 34–46.

Stockli, R., Rutishauser, T., Baker, I., Liniger, M.A., Denning, A.S., 2011. A global reanalysis of vegetation phenology. J. Geophys. Res. 116, G03020, http://dx.doi.org/10.1029/2010JG001545.

Stoy, P., et al., 2013. A data-driven analysis of energy balance closure across FLUXNET research sites: the role of landscape scale heterogeneity. Agric. For. Meteorol. 171–172, 137–152.

Stromberg, J.C., 2001. Restoration of riparian vegetation in the south-western United States: importance of flow regimes and fluvial dynamism. J. Arid Environ. 49, 17–34.

Syed, K.H., Flanagan, L.B., Carlson, P.J., Glenn, A.J., Van Gaalen, K.E., 2006. Environmental control of net ecosystem CO_2 exchange in a treed: moderately rich fen in northern Alberta. Agric. For. Meteorol. 140, 97–114.

Vörösmarty, C.J., McIntyre, P.B., Gessner, M.O., Dudgeon, D., Prusevich, A., Green, P., Glidden, S., Bunn, S.E., Sullivan, C.A., Reidy Liermann, C., Davies, P.M., 2010. Global threats to human water security and river biodiversity. Nature 467, 555–561.

Wang, K., Dickinson, R.E., 2012. A review of global terrestrial evapotranspiration: observation, modeling, climatology, and climatic variability. Rev. Geophys. 50 (RG2005).

Wever, L.A., Flanagan, L.B., Carlson, P.J., 2002. Seasonal and interannual variation in evapotranspiration: energy balance and surface conductance in a northern temperate grassland. Agric. For. Meteorol. 112, 31–49.

Williams, C.A., Cooper, D.J., 2005. Mechanisms of riparian cottonwood decline along regulated rivers. Ecosystems 8, 382–395.

Wilson, K., et al., 2002. Energy balance closure at FLUXNET sites. Agric. For. Meteorol. 113, 223–243.

Wong, S.C., Cowan, I.R., Farquhar, G.D., 1979. Stomatal conductance correlates with photosynthetic capacity. Nature 282, 424–426.

Zha, T., Barr, A.G., van der Kamp, G., Black, T.A., McCaughey, J.H., Flanagan, L.B., 2010. Interannual variation of evapotranspiration from forest and grassland ecosystems in western Canada in relation to drought. Agric. For. Meteorol. 150, 1476–1484.